Miner Petrol
DOI 10.1007/s00710-017-0502-6

ORIGINAL PAPER

Geochemistry and mineral chemistry of pyroxenite xenoliths and host volcanic alkaline rocks from north west of Marand (NW Iran)

Ali Akbar Khezerlou[1] · **Nasir Amel**[1] · **Michel Gregoire**[2] · **Mohsen Moayyed**[1] · **Ahmad Jahangiri**[1]

Received: 29 August 2016 / Accepted: 16 February 2017

Abstract The Plio-Quaternary alkaline volcanic rocks from the northwest of Marand (NW Iran) consist of trachy-andesites, trachy-basaltic andesites, leucite-tephrites and tephrites. They display a distinct LILE and LREE enrichment, a HFSE depletion (Ta, Ti, and Nb) and high Ba/Ta and Ba/Nb ratios, which are among the characteristics of subduction-derived magmatic rocks. The investigated clinopyroxenite xenoliths mostly occur within the trachy-andesites and more rarely within the trachy-basaltic andesite rocks. These xenoliths, which have a cumulate texture, are classified into four groups based on their mineralogical and chemical features. Group 1 contains clinopyroxene and amphibole as the main minerals. This group does not indicate a clear enrichment in incompatible trace elements in contrast with the Groups 2 and 4, where Ba, Th and U are enriched. Major element contents of clinopyroxenes and amphiboles of Group 1 xenoliths are similar to those of their counterparts of intermediate volcanic rocks. In addition, their contents of compatible elements such as Cr and Ni (whole rock) are also the same, implying a similar magmatic origin. Group 2 contains clinopyroxene and phlogopite as the main minerals. This group, similarly to potassic and ultrapotassic volcanic rocks, is enriched in LREE compared to HREE and unlike the intermediate volcanic rocks, does not contain amphibole. Their $^{143}Nd/^{144}Nd$ and $^{86}Sr/^{87}Sr$ ratios are also different. Given the Cr and Ni contents, the REE pattern shape and the chemical composition of clinopyroxene and phlogopite, it seems that the parental melt of this group is similar to the one of potassic and ultrapotassic volcanic rocks. Group 3 contains clinopyroxene and biotite as the main minerals. The REE pattern of this group, unlike those of Groups 1, 2 and 4, has a relatively flat slope. In addition, the content of compatible elements, such as Cr and Ni, also differ as well as the chemical composition of clinopyroxene and mica, which are also different from those of volcanic rocks. Group 4 clinopyroxenites contain clinopyroxene, phlogopite and amphibole as the main minerals. The LREE-enriched patterns and the Ba, U and Pb enrichment of this group are similar to those of the Group 2. The samples of this group on the other hand differ from those of the Group 2 clinopyroxenites in terms of crystal size, crystallization depth, Cr and Ni contents, and chemical composition of clinopyroxene. The parental melt of this group is similar to that of the intermediate volcanic rocks.

Keywords Iran · Marand · Trachy-andesite · Pyroxenite xenoliths · Cumulate texture

Editorial handling: L. Fedele

Electronic supplementary material The online version of this article (doi:10.1007/s00710-017-0502-6) contains supplementary material, which is available to authorized users.

✉ Ali Akbar Khezerlou
ali.khezerlou2@gmail.com

[1] Department of Geology, University of Tabriz, Tabriz 51664, Iran

[2] Laboratory Geosciences Environnement Toulouse, CNES-CNRS-IRD-UPS Midi-Pyrenees Observatory, Toulouse University, 14 Av. E. Belin, 31400 Toulouse, France

Introduction

Iran is an active tectonic area belonging to the Alpine-Himalayan orogenic belt. Neotethys oceanic plate was subducted beneath the Iranian continental crust during Middle Cretaceous (Ghasemi and Talbot 2006) and the process ended in the Late Cretaceous (Coleman 1971; Ricou 1971; Berberian and King 1981; Whitechurch et al. 1984; Boudier et al. 1988; Nicolas 1989; Searle and Cox 1999). The resulting collision of the

Published online: 28 February 2017

Iranian continental plate and the African-Arabian continental plate caused the evolution of the following structural zones: Folded Zagros (High Zagros and Folded Zagros Belt), the Metamorphic Sanandaj-Sirjan zone and the Urumieh-Dokhtar Magmatic Arc (UDMA) form the original NW-SE directed Zagros orogenic belt (Alavi 1994; Ghasemi and Talbot 2006). In UDMA, several volcanic events occurred during the Neogene, reaching a maximum intensity during the Eocene (e.g. Stöcklin 1974; Farhoudi 1978; Emami 1981; Alavi 2004). The alkaline volcanic rocks to the northwest of Marand with Plio-Quaternary age are located in the northern UDMA (Fig. 1). The investigated pyroxenite xenoliths occur in these volcanic rocks.

Pyroxenites commonly form at lower crustal or upper mantle depths, and occur as xenoliths of variable sizes in volcanic rocks, providing valuable information about the nature and evolution of the upper mantle and lower crust (Downes 1993; Griffin et al. 1999; Nasir et al. 2006). Previous studies have reported pyroxenite xenoliths transported by alkaline melts from different localities worldwide (e.g. Bondi et al. 2002; Xu 2002; Egorova et al. 2006; Ackerman et al. 2012; Saadat and Stern 2012; Ying et al. 2013; Platevoet et al. 2014). In this study, we present the petrological, mineralogical and geochemical (including isotopic Sr and Nd ratios) data of clinopyroxenite rocks from northwestern Marand, in order to better understand their petrogenesis and the implications for the magmatic history of the investigated area. In addition, mineral chemistry and whole rock geochemical data are used to link the parental melts of pyroxenite xenoliths and volcanic rocks.

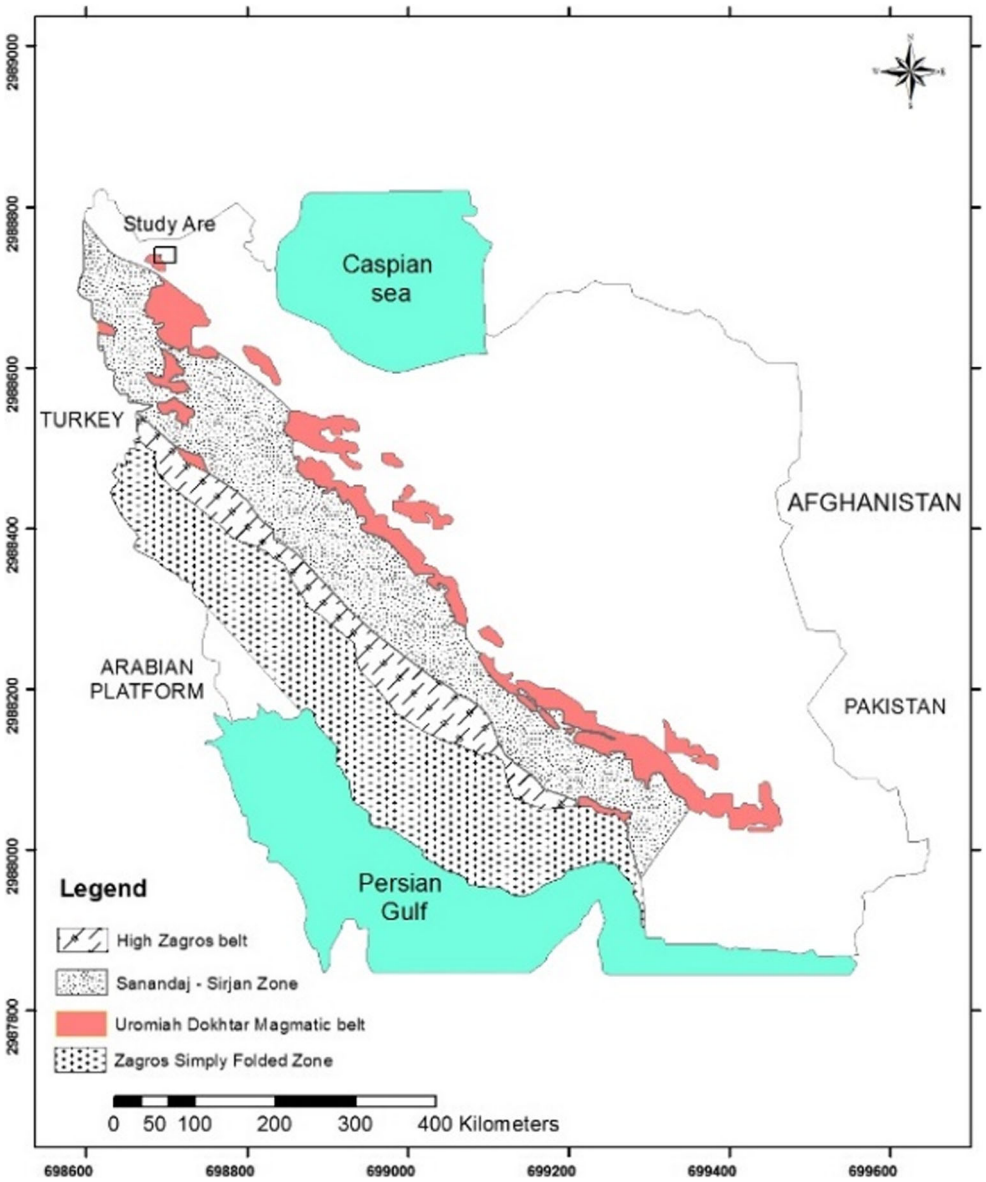

Fig. 1 The four main tectonic units of the Zagros orogenic belt (after Alavi 1994; modified from Ghasemi and Talbot 2006)

Geological setting

The study area is part of the Pliocene-Quaternary volcanic province of North West Iran, which is itself part of a Neogene-Quaternary magmatic belt (Stöcklin 1977). The most important structures of this area are the Divan Daghi and Gharagoz Mountains, located respectively to the northwest and to the northeast of the study area, the North Tabriz Fault, occurring between the Mishu mountain and the Pliocene-Quaternary volcanic province from the northwest of Marand city, and finally the Divan Daghi Fault, located south of the Divan Daghi Mountain. The Divan Daghi and Gharagoz Mountains, and the eastern and western parts of the Mishu Mountain, are elevated regional structures (pop up) related to the activity of the Tabriz faults; i.e. the South Mishu Faults, the Tasuj Fault (TsF) and the South Fault of Divan Daghi. The A_2-type granitoids at Mishu and the Hercynian mafic-ultramafic rocks from the eastern Mishu Mountains are witnesses of the Paleotethys Suture Zone (Moayyed and Moazzen 2002; Moayyed and Hosseinzadeh 2012; Ahankoub et al. 2013). In the western Mishu Mountains Oligocene to upper Miocene sediments are exposed. The Divan Daghi and Gharagoz Mountains are characterized by outcrops of Paleozoic and Mesozoic volcanic rocks with acidic components, and also by A_2-type granitoids of Hercynian age. The Permo-Triassic sediments of the Jolfian Formation and the Jurassic sediments were thrust over the Marand Pliocene-Quaternary Volcanic Province (study area) from the south, and thrust over the siliciclastic red bed sediments of Miocene age from the north. Volcanic activity in the northwestern Marand province started with eruptions of high potassium calc-alkaline andesitic pyroclastic rocks, and gradually evolved to SiO_2-undersaturated potassic–ultrapotassic, mostly shoshonitic, eruptions (Khezerlou et al. 2008; Ahmadzadeh et al. 2010). The upper Miocene deposits are covered by these volcanic rocks, and therefore the stratigraphic age of the latter must be younger than upper Miocene. Leucite-tephrite, tephrite, trachy-basaltic andesite, trachy- andesite lavas and lamprophyric dykes occur in the study area (Fig. 2). Similar rocks (8–11 Ma) also outcrop in the Islamic peninsula (Moradian et al. 1997; Pang et al. 2013; Shafaii Moghadam et al. 2013). The xenoliths consist of pyroxenites, amphibolites, gabbros, diorites, lamprophyres and hornfels. They mostly occur in variable proportion everywhere in the study area in the trachy-andesite and rarely in trachy-basaltic andesites. Pyroxenite and amphibolite are more abundant than other xenolith types. The size of the xenoliths is highly variable, most of them ranging from 2 to 5 cm, but some samples reach up to 10 cm in size. In the vicinity of North Tabriz Fault and South Divan Daghi Fault subvolcanic andesitic, trachyandesitic, dacitic and rhyodacitic domes with shoshonite affinity outcrop along a NW-SE directed zone. These domes are injected into clastic red bed sediments of Miocene age (Jahangiri 2007). The relationships of these rocks with the potassic-ultrapotassic rocks from the volcanic province located northwest of Marand remain unknown. Recently Bazargani (2014) studied the Tabakh Daghi region, and reported that one of these domes is injected into potassic-ultrapotassic lavas, inferring that the domes are probably younger than 8–11 million years. Amphibolite xenoliths are also abundant in these domes.

Petrography of volcanic rocks

Volcanic rocks of the study area are intermediate (trachy-andesite and trachy-basaltic andesite) and potassic-ultrapotassic (leucite-tephrite and tephrite) in composition.

Intermediate rocks

The majority of xenoliths from the study area occur in trachy-andesites and more rarely in the trachy-basaltic andesite rocks. The main minerals of these volcanic rocks are plagioclase and clinopyroxene, while mica (phlogopite and biotite), amphibole, opaques, K-feldspar and apatite are the minor minerals. The rocks show porphyritic and microlithic-porphyritic textures (Fig. 3c, d). Plagioclase modal content in trachy-andesite (45–55%) is slightly higher than in trachy-basaltic andesite (40–45%). Plagioclase forms euhedral to subhedral crystals occurring either as very fine microliths within the matrix or as zoned crystals larger than 3 mm (Fig. 3c). Some plagioclase phenocrysts have sieved texture (Fig. 3d). Euhedral to subhedral clinopyroxenes occur as phenocrysts 1–3 mm in size (modal content: 8–10%) in trachy-andesites. Although clinopyroxene modal content in the trachy-basaltic andesites is much higher (15–18%), it remains lower than that of plagioclases phenocrysts. No clinopyroxene microliths have been observed in the matrix of the trachy-andesite, but some occur in the matrix of the trachy-basaltic andesite (Fig. 3d). Some clinopyroxene phenocrysts display zoning and sieved texture. Most trachy-basaltic andesites show poikilitic texture, where fine opaques, apatite and mica crystals are observed inside clinopyroxene phenocrysts. The euhedral mica and amphibole phenocrysts, 0.5 to 1 mm in size, occur in the matrix and compose 5–8% of the samples. Some mica and amphiboles display opacitization (Fig. 3c). Apatite crystals occur as euhedral small inclusions inside other minerals (particularly clinopyroxene) and in the matrix. The matrix is composed of plagioclase, sanidine, opaque minerals and glass.

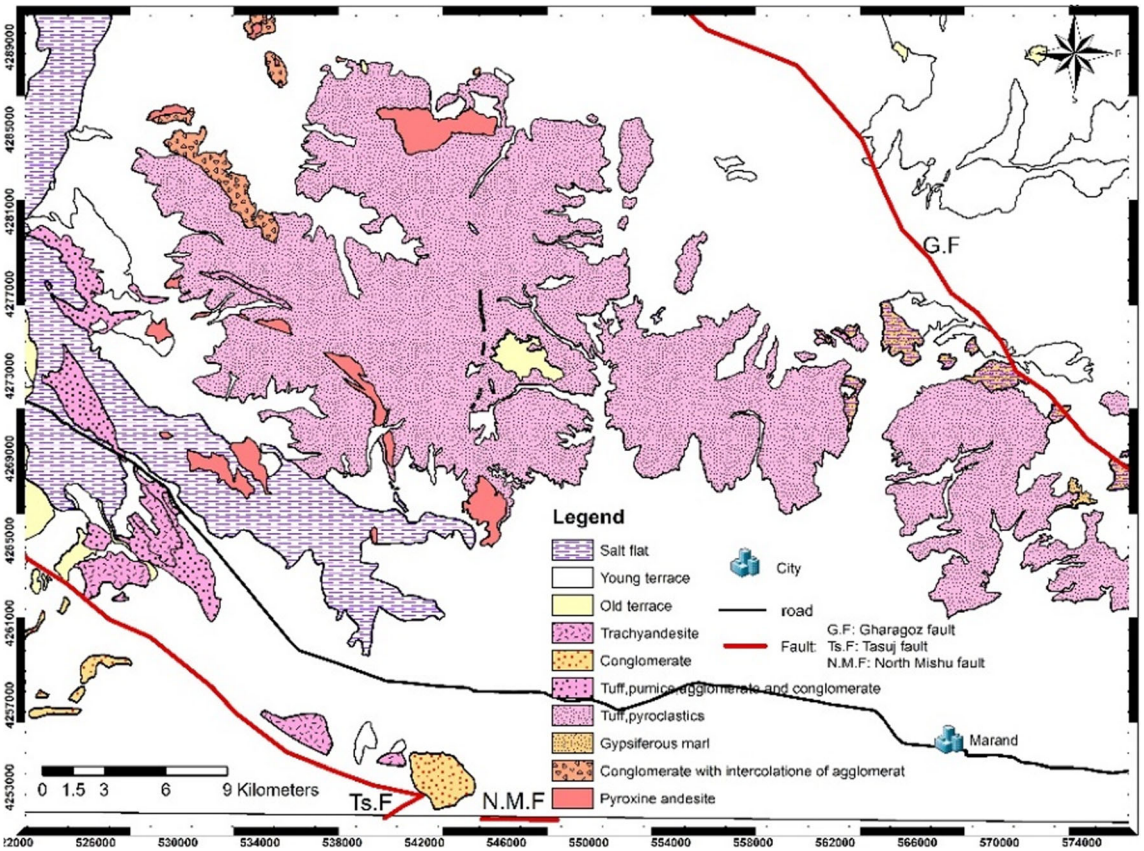

Fig. 2 Geological map of the study area. (simplified from the geological maps of 1:100,000 Marand, Jolfa, Gharezyaadin and Tasuj)

Potassic and ultrapotassic volcanic rocks

These rocks do not contain xenoliths and are mostly leucite-tephrites and tephrites consisting of clinopyroxene, plagioclase, and leucite as the main minerals associated with mica, apatite, and opaques as the minor minerals. They mostly have porphyritic texture (Fig. 3a, b). Euhedral to subhedral clinopyroxenes occur as coarse phenocrysts (1–3 mm) and smaller crystals in the matrix (Fig. 3a, b). The modal content of clinopyroxene in leucite-tephrite (20–25%) is higher than in tephrite (10–15%). Euhedral and subhedral plagioclases are observed as phenocrysts and smaller crystals in these rocks (Fig. 3a, b). They display a lower modal content in the leucite-tephrite (10–15%) than in the tephrite (15–20%).

Leucite is the main mineral in the leucite-tephrite, and occurs as coarse (1–2 mm) to small euhedral phenocrysts (Fig. 3a), while it is observed in tephrite only as minor small crystals (Fig. 3b). Leucite modal content in leucite-tephrite (10–15%) is therefore higher than in the tephrite (5–8%). The matrix in these rocks consists of plagioclase, clinopyroxene, apatite, opaque minerals, mica and glass. Apatite content in the potassic and ultrapotassic volcanic rocks is higher than that of intermediate volcanic rocks.

Petrography of clinopyroxenite xenoliths

Mineral modal abundances were estimated by point counting under a polarizing microscope. Clinopyroxenite xenoliths from the study area consist of coarse grained pieces of rocks with glossy black color and sharp edges surrounded by the volcanic host rock in hand samples. These xenoliths for the major part have ellipsoid shape with diameter ranging from 2 to 12 cm. They all display a cumulate texture (Fig. 3c-h). Based on the nature of the main minerals coexisting with clinopyroxene, these xenoliths can be classified into four groups. In Groups 1 to 4, clinopyroxene is observed with amphibole, phlogopite, biotite, and amphibole and phlogopite, respectively.

Group 1 consists only of the sample K-3. The main minerals are clinopyroxene and amphibole with opaques and apatite as minor minerals. This clinopyroxenite displays an orthocumulate texture. The euhedral and subhedral clinopyroxenes (as cumulus phase) 0.2–1.5 mm in size make up to 70% of the sample. Small opaque minerals and apatite are observed as inclusions inside the clinopyroxenes (poikilitic texture). The anhedral to subhedral amphiboles (as intercumulus phase), 0.3 to 2 mm in size and making up 25% of the sample, is the only hydrous mineral.

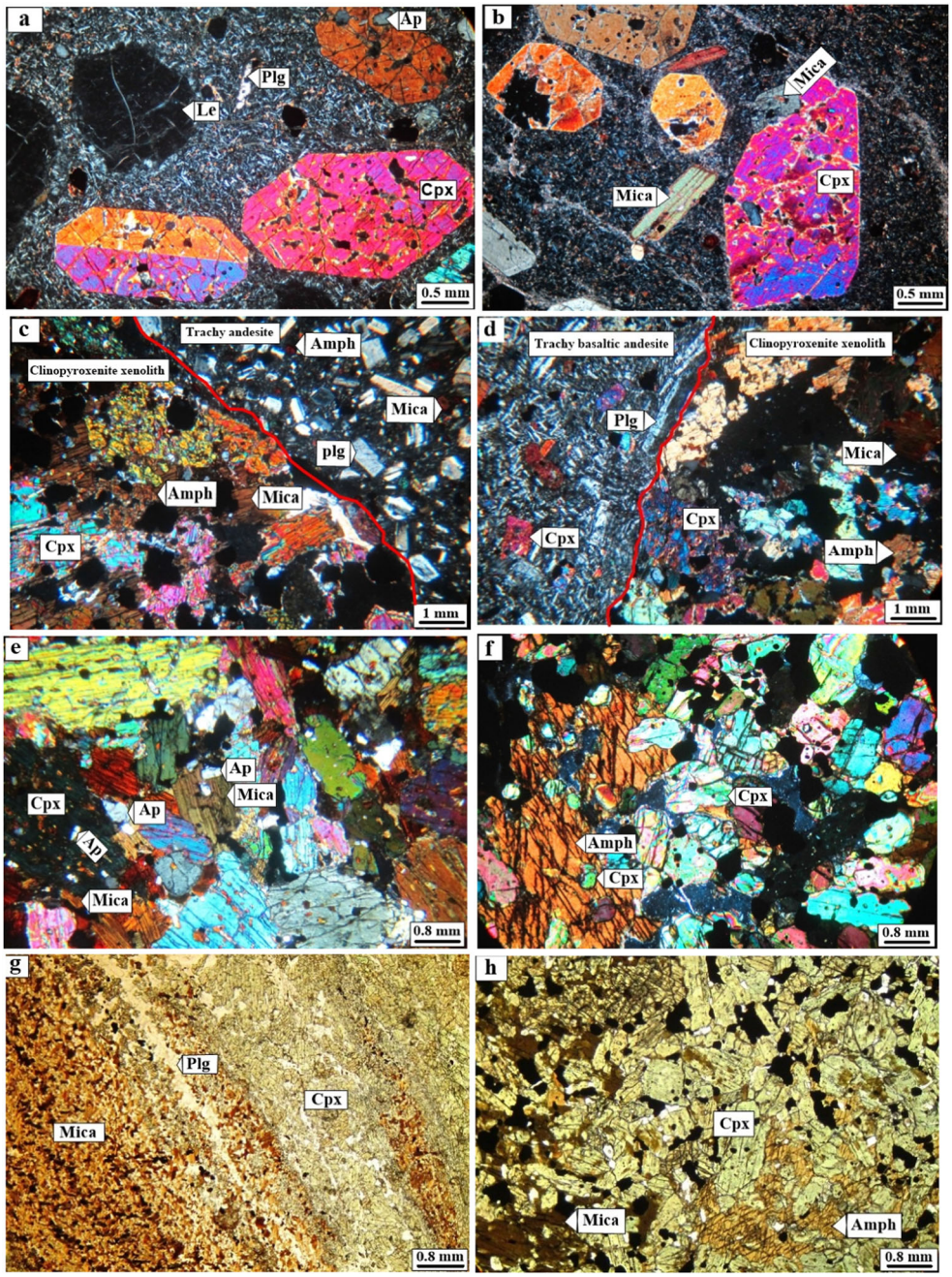

Fig. 3 Photomicrographs of volcanic rocks and clinopyroxenite xenoliths from the study area: **a** plagioclase (Plg), clinopyroxene (Cpx), apatite (Ap) and leucite (Le) phenocrysts in leucite-tephrite, crossed polars (XPL); **b** Clinopyroxene and mica phenocrysts in tephrite, XPL; **c** Plagioclase, mica and amphibole (Amph) phenocrysts in trachy-andesite and clinopyroxenite with clinopyroxene and mica as cumulus phases and amphibole as intercumulus phase, Xpl; **d** Plagioclase and clinopyroxene phenocrysts in trachy-basaltic andesite and clinopyroxenite with clinopyroxene and mica as cumulus phases and amphibole as intercumulus phase, XPL; **e** Clinopyroxenite with clinopyroxene and mica as cumulus phases, XPL; **f** Clinopyroxenite with clinopyroxene (as cumulus phase) and amphibole as intercumulus phase, XPL; **g** Clinopyroxenite with clinopyroxene as cumulus phase and biotite (Bt) and plagioclase as intercumulus phases, plane parallel polars (PPL); **h** Clinopyroxenite with clinopyroxene and mica (as cumulus phases) and amphibole as intercumulus phase, PPl

Finally, some clinopyroxene and opaque minerals are surrounded by amphiboles (Fig. 3f).

Group 2 consists of samples kh-14, kh-62 and kh-64, which have clinopyroxene and phlogopite as main minerals and opaques and apatite as minor minerals. These clinopyroxenites have adcumulate texture. Clinopyroxenes (as cumulus phase) occur as euhedral to subhedral crystals, and their modal content ranges from 70 to 75%. These clinopyroxenes are coarser (1.5 to 3 mm in size) than those of Group 1 (Fig. 3e). Phlogopite (as cumulus phase) modal content in Group 2 xenoliths varies from 20 to 25%. Its size ranges from 0.1 mm to crystals >1.5 mm, with some of the smaller phlogopites observed as inclusions within clinopyroxene. In this group amphibole is missing and the apatite modal content is higher than in the other groups. Some apatites, similarly to phlogopite and opaques, are observed as inclusions in poikilitic clinopyroxene (Fig. 3e).

Group 3 consists of the k-33 sample, which contains clinopyroxene and biotite as the main minerals, and opaques and plagioclase as the minor minerals. This clinopyroxenite exhibits orthocumulate texture. Clinopyroxene is a cumulus phase, 0.1–0.2 mm in size, which makes up 50% of the modal

content. Biotite (< 0.05 mm in size) is an intercumulus phase, which constitutes 40% of the modal content. Clinopyroxene and biotite occur as alternating layers. Plagioclase (< 0.3 mm in size) is an intercumulus phase that constitutes 8% of the modal content. It occurs as small crystals near the clinopyroxenes. This sample lacks apatite but contains some opaque minerals (Fig. 3g).

Group 4 consists of samples kh-7, kh-87, k-40, and kh-93. Clinopyroxene, phlogopite, and amphibole are the main minerals, while apatite and opaques are the minor ones. The texture of this Group is similar to groups 1 and 3. Clinopyroxene, apatite and phlogopite are the cumulus phases, while amphibole occurs as intercumulus phase. Group 4 clinopyroxene (1–2 mm) is larger than that of Groups 1 and 3, but smaller than those of Group 2. The clinopyroxene modal content ranges from 60 to 70%. Amphibole and phlogopite, ranging in size from 0.2 to 1.2 mm, both constitute 25–30% of the modal content of Group 4. The content of opaque minerals in this group is higher than in Groups 1 to 3. Indeed, apatite and opaque minerals constitute 6–9% of the modal content and are less than 0.3 mm in size. Some samples of this group, similarly to Group 2, show poikilitic texture, where small opaque phases, apatite and phlogopite crystals are observed within clinopyroxenes. Finally, some of the clinopyroxenes are surrounded by amphiboles (Fig. 3c–h).

Analytical methods

The major element compositions of minerals were acquired at the "Centre de Micro Caractérisation Raimond Castaing" (CNRS, University Toulouse III, INPT, INSA, Toulouse, France), using a Cameca SXFive electron microprobe. The operating conditions were as follows: accelerating voltage 15 kV; beam current 20 nA; analysed surface around 2 × 2 μm^2. The following standards were used: albite (Na), periclase (Mg), corundum (Al), sanidine (K), wollastonite (Ca, Si), pyrophanite (Mn), hematite (Fe), Cr_2O_3 (Cr), NiO (Ni) and sphalerite (Zn).

The bulk rock major and minor elements were analyzed using an Inductively Coupled Plasma Atomic Emission Spectrometer (ICP AES) Horiba Jobin Yvon Ultima 2 at the "Pôle de Spectrométrie Océan" (PSO/IUEM, Plouzané, France), following the protocol adapted from Cotten et al. (1995). Each powdered sample was digested in Teflon vials with HF 32 N and HNO_3 14.4 N and the dry residue was dissolved in a H_3BO_3 solution. WSE and ACE internationals standards were used as internal and external control. The precision of measurements performed on that instrument is usually better than 1% for both SiO_2 and TiO_2, 2% for Al_2O_3 and Fe_2O_3, and better than 4% for the other major oxides.

Trace element concentrations were determined using a High Resolution Inductively Coupled Plasma Mass Spectrometer (HR ICP-MS) Thermo Finnigan Element II ("Pôle de Spectrométrie Océan" PSO/IUEM, Plouzané, France), following a method adapted from Barrat et al. (2007). About 100 mg of sample were digested in Teflon vials within distilled HF 32 N and HNO_3 14.4 N. The dry residue was dissolved in HNO_3 14.4 N and then in HCl 3 N. An aliquot of the solution was diluted in HNO_3 0.3 N and spiked with Tm spike. BCR2 and BEN were used as external control and BHVO-2 was used for internal control. The precision of measurements was better than 5% for all elements.

Samples were also analyzed for Sr and Nd radiogenic isotopes. About 200 mg of sample material was weighted and dissolved in savillex beakers in a mixture of ultrapure distilled HF (24 N), and HNO_3 (14 N) for four days at 120 °C on a hot plate. Sr and Nd fractions were chemically separated using the Eichrom specific resins TRU-spec, Sr-spec and Ln-spec following conventional column chemistry procedure (Pin and Santos Zalduegui 1997). The Sr and Nd isotope compositions were measured in static mode on a Thermo TRITON spectrometer at the PSO (IUEM, Plouzané, France). All measured Sr and Nd ratios were normalized to $^{86}Sr/^{88}Sr = 0.1194$ and $^{146}Nd/^{144}Nd = 0.7219$, respectively and $^{87}Sr/^{86}Sr$ values were normalized to the recommended value of NBS987 (0.710250). During the course of analysis, Nd standard solution La Jolla gave 0.511859 ± 2 (n = 2, recommended value 0.511850) and JNdi gave 0.512117 ± 3 (n = 1, recommended value 0.512100).

Chemistry of minerals

Eight clinopyroxenites were analyzed using the electron microprobe technique. For samples kh-7 and kh-87, the constituent minerals of the host volcanic rock and xenoliths were analyzed, while for samples k-3, k-40, kh-62, kh-64, kh-14 and k-33 only the constituent minerals of xenoliths were analyzed.

Mica

As shown in Fig. 4a, phlogopite occurs in Group 2 and 4 clinopyroxenites. Mg# ($Mg/Mg + Fe^{2+}$) in kh-40, kh-7 and kh-87 Group 4 samples (0.64–0.69) is lower than in the kh-62, kh-64 and kh-14 Group 2 samples (0.74–0.77). In Group 2 SiO_2 and FeOt contents of phlogopites are lower and MgO contents are higher than in Group 4 phlogopites, respectively (Table 1 and Electronic Appendix 1). In samples kh-64 (Group 2) and k-40 (Group 4), element concentrations do not show large variation from core to rim. Only a limited normal zoning is observed, corresponding from core to rim

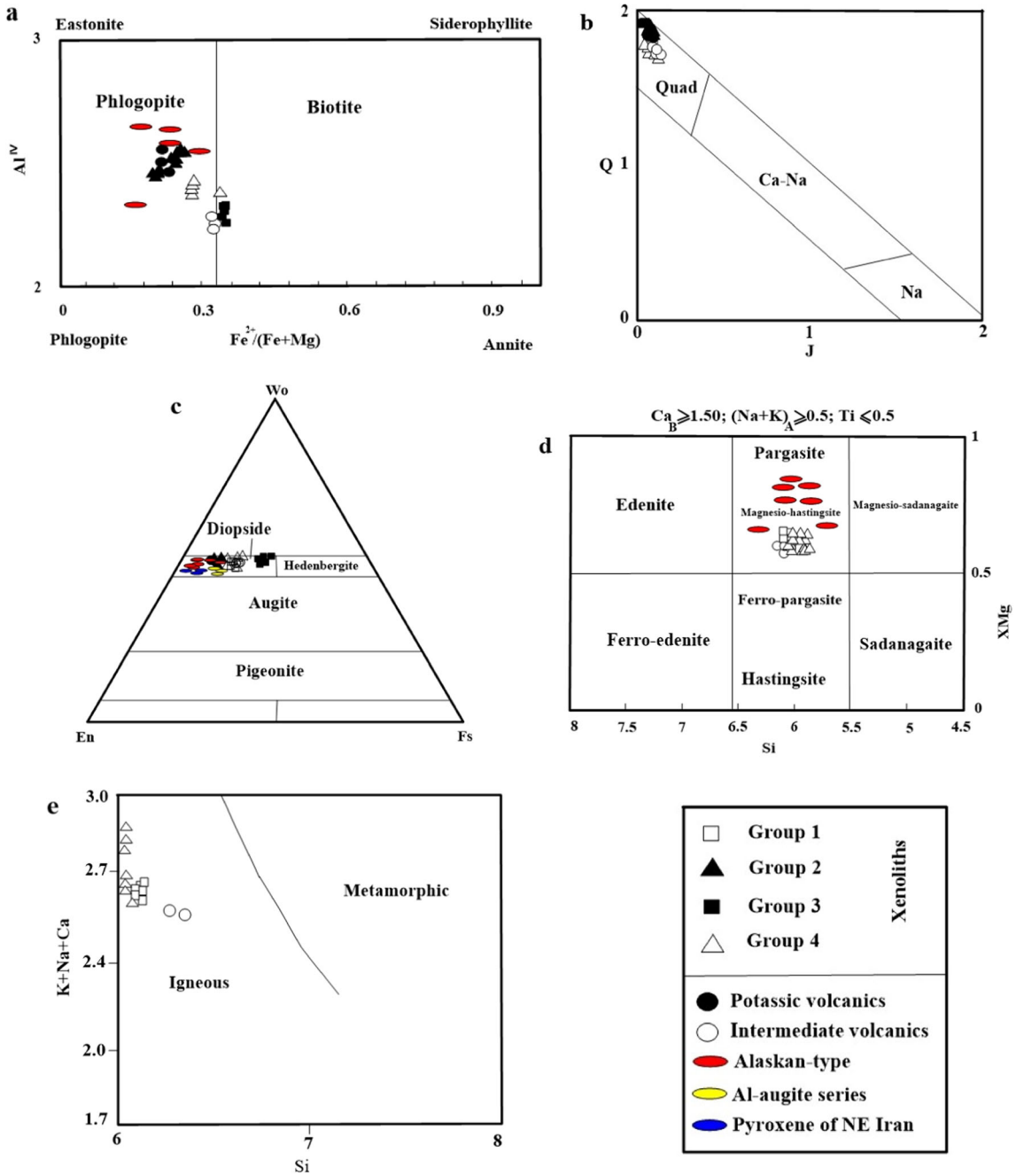

Fig. 4 **a** Classification of micas (Speer 1984), **b** Composition of clinopyroxenes in the Q-J diagram (J = 2Na, Q = Ca + Mg + Fe^{2+}), **c** Classification of clinopyroxenes (Morimoto et al. 1988), **d** Classification of amphiboles (Leake et al. 1997), **e** Plot of Si versus K + Na + Ca for amphiboles from the volcanic rocks and clinopyroxenite xenoliths

to an increase of SiO_2 content and a decrease of MgO and TiO_2 contents. In phlogopite of sample DL13, a potassic volcanic rock, the FeO content increases while MgO, Al_2O_3 and TiO_2 decrease from core to rim. The micas in the Group 3 sample are biotites (Fig. 4a) with Mg# 0.63–0.66 and higher Na_2O, FeOt, and Cr_2O_3 and lower MgO and TiO_2 contents than phlogopites of Groups 2 and 4 (Table 1 and Electronic Appendix 1). The TiO_2 content for Group 4 micas is respectively higher and lower than that for Group 3 and Group 2. In Fig. 4a, the micas of Group 2 appear to be similar to those of potassic and ultrapotassic volcanic rocks while micas in Group 4 plot close to those of the intermediate volcanic rocks. Moreover, SiO_2, MgO, and FeOt contents of phlogopites from kh-40, kh-7 and kh-87 Group 4 clinopyroxenites are similar to those of phlogopites from intermediate volcanic rocks, while those of kh-62, kh-64 and kh-14 Group 2 clinopyroxenites are similar to those of phlogopites from potassic and ultrapotassic volcanic

Table 1 Mineral chemical composition of micas in clinopyroxenite xenoliths and volcanic rocks (IVR = Intermediate volcanic rocks)

Rock	Group 2						Group 3		Group 4			IVR	Potassic volcanics[a]	
Sample	kh-14	kh-14	Kh-62	Kh-62	kh-64	kh-64	k-33	k-33	Kh-7	K-40	K-40	v-Kh-7	DL13	DL13
Location	Core	Core	Core	Core	Core	Rim	Core	Core	Core	Core	Rim	Core	Core	Rim
SiO_2	35.86	35.88	36.82	36.49	36.73	36.76	37.97	37.55	37.05	36.78	36.64	37.36	35.9	35.39
TiO_2	5.51	5.69	5.45	5.14	5.25	5.23	1.99	1.98	5.14	4.09	4.13	5.5	6.83	5.92
Al_2O_3	14.44	14.65	14.47	14.3	14.76	14.65	14.23	14.18	13.52	14.93	14.36	12.85	14.76	14.22
Cr_2O_3	0.05	0.03	0.04	0.04	0.06	0.03	0.16	0.19	0.00	0.01	0.01	0.02	0.00	0.00
FeOt	9.92	9.76	9.32	9.99	10.24	10.44	14.49	14.66	14.72	13.02	12.51	15.51	9.73	11.54
MnO	0.06	0.06	0.03	0.06	0.03	0.04	0.21	0.18	0.32	0.13	0.11	0.34	0.09	0.18
MgO	16.73	16.73	17.16	17.13	17.02	16.80	15.74	15.63	14.48	15.60	15.50	14.15	17.19	15.87
CaO	0.00	0.01	0.01	0.00	0.02	0.04	0.10	0.17	0.05	0.17	0.21	0.01	0.05	0.81
Na_2O	0.54	0.51	0.50	0.63	0.55	0.50	0.75	0.68	0.54	0.39	0.45	0.69	0.50	0.73
K_2O	8.76	8.54	8.85	8.84	8.65	8.87	8.45	8.14	8.85	7.97	8.16	8.87	8.53	8.03
Total	91.87	91.86	92.65	92.62	93.31	93.36	94.09	93.36	94.67	93.09	92.08	95.3	93.58	92.69
	Cations calculated on the basis of 22 oxygens													
Si	5.44	5.43	5.51	5.49	5.48	5.49	5.72	5.70	5.58	5.54	5.58	5.61	5.33	5.37
Al (IV)	2.56	2.57	2.49	2.51	2.52	2.51	2.28	2.30	2.40	2.46	2.42	2.27	2.58	2.54
Al (VI)	0.02	0.04	0.06	0.02	0.07	0.07	0.24	0.23	0.00	0.19	0.16	0.00	0.00	0.00
Ti	0.63	0.65	0.61	0.58	0.59	0.59	0.23	0.23	0.58	0.46	0.47	0.62	0.76	0.68
Fe^{2+}	1.26	1.23	1.17	1.26	1.28	1.30	1.82	1.86	1.85	1.64	1.59	1.95	1.21	1.46
Mn	0.01	0.01	0.00	0.00	0.00	0.00	0.03	0.02	0.04	0.02	0.01	0.04	0.01	0.02
Mg	3.78	3.77	3.83	3.84	3.78	3.74	3.53	3.54	3.25	3.5	3.52	3.17	3.81	3.59
Ca	0.00	0.00	0.00	0.00	0.00	0.01	0.02	0.03	0.01	0.03	0.03	0.00	0.01	0.13
Na	0.16	0.15	0.14	0.18	0.16	0.15	0.22	0.2	0.16	0.11	0.13	0.2	0.14	0.21
K	1.69	1.65	1.69	1.70	1.65	1.69	1.62	1.58	1.70	1.53	1.58	1.70	1.62	1.55
#mg	0.75	0.75	0.77	0.75	0.75	0.74	0.66	0.66	0.64	0.68	0.69	0.62	0.76	0.71

[a] Data for potassic and ultrapotassic volcanic rocks are from Ahmadzadeh et al. (2010)

rocks (Table 1 and Electronic Appendix 1). We have compared micas in xenoliths of the study area with micas in clinopyroxenites of Alaskan-type massifs from southeastern Alaska (Himmelberg and Loney 1995). As shown in Fig. 4a, the micas of Alaskan-type massifs are phlogopites characterized by higher Al_2O_3, MgO, SiO_2 and K_2O and lower TiO_2 and Na_2O contents than those of the investigated Groups 2 and 4 clinopyroxenites. Micas in the Group 3 clinopyroxenite xenolith have higher FeOt, MnO and Na_2O and lower K_2O, Al_2O_3 and MgO contents, compared to the Alaskan-type phlogopites.

Clinopyroxene

In the classification scheme proposed by Morimoto and Kitamura (1983), the analyzed clinopyroxenes plot in the field of Quad (Ca-pyroxene) (Fig. 4b). The clinopyroxene of all the clinopyroxenite xenoliths plot in the diopside field (Fig. 4c) and have a Mg# varying from 0.66 to 0.84 (Table 2 and Electronic Appendix 2). The core and rim of clinopyroxene from Group 2 and 4 clinopyroxenites have an almost homogenous composition, with only a slight increase in SiO_2 and decrease in MgO and TiO_2 in rim compared to core. The variation of major element contents is almost negligible for clinopyroxenes within all the investigated samples, but sample k-40 from Group 4. In the latter there is indeed a large difference in SiO_2, FeOt, MgO, TiO_2 and Al_2O_3 contents. Clinopyroxenes of kh-7, kh-87, k-40 Group 4 samples and k-3 Group 1 sample have higher SiO_2 and FeO and lower MgO contents compared to those of Group 2 samples. The clinopyroxenes of the intermediate and potassic-ultrapotassic volcanic rocks are also diopsides. The SiO_2, Al_2O_3, MgO, and FeO_t contents in clinopyroxenes of Group 1 and Group 4 clinopyroxenites are similar to those of intermediate volcanic rocks (samples v-kh-7 and v-kh-87), while those of clinopyroxenes of Group 2 samples are similar to those of potassic and ultrapotassic volcanic rocks (Table 2 and Electronic Appendix 2). The composition of clinopyroxene of the Group 3 clinopyroxenite k-33 differs from the other clinopyroxenites. Indeed this clinopyroxene also plots in the diopside field but closer to the hedenbergite

Table 2 Mineral chemical composition of clinopyroxenes in clinopyroxenite xenoliths and volcanic rocks

Rock	Group 1			Group 2							Group 3		
Sample	k-3	k-3	k-3	kh-14	kh-14	kh-62	kh-62	kh-64	kh-64	kh-64	k-33	k-33	k-33
Location	Core	Core	Core	Core	Core	Core	Core	Core	Mantle	Rim	Core	Core	Core
SiO_2	49.09	49.73	49.95	52.78	52.47	52.54	52.47	52.23	52.14	52.3	50.53	51.74	51.01
TiO_2	1.06	0.98	0.99	0.51	0.63	0.55	0.69	0.7	0.76	0.61	0.1	0.06	0.16
Al_2O_3	4.33	4.06	4.11	2.25	2.65	2.51	2.20	2.50	2.25	2.16	1.34	0.73	1.35
Cr_2O_3	0.00	0.00	0.00	0.06	0.03	0.01	0.03	0.04	0.02	0.04	0.00	0.05	0.41
FeOt	8.26	8.60	8.44	6.58	6.93	6.66	6.57	6.99	6.86	6.68	15.44	12.75	12.8
MnO	0.21	0.15	0.25	0.22	0.25	0.22	0.23	0.13	0.24	0.08	0.78	0.76	0.70
MgO	12.44	12.19	12.24	15.00	14.76	15.01	13.73	13.54	13.80	13.88	8.17	9.39	9.76
CaO	22.82	22.89	22.99	21.67	21.94	21.95	23.38	23.17	23.10	23.10	23.49	23.63	23.61
Na_2O	0.56	0.56	0.62	0.49	0.53	0.51	0.51	0.64	0.53	0.49	0.19	0.17	0.26
K_2O	0.00	0.00	0.02	0.00	0.00	0.01	0.01	0.00	0.00	0.01	0.00	0.01	0.02
Total	98.776	99.203	99.619	99.57	100.26	100.11	99.85	99.98	99.7	99.35	100.183	99.307	99.734
	Cations calculated on the basis of 6 oxygens												
Si	1.85	1.87	1.87	1.95	1.93	1.94	1.95	1.94	1.94	1.95	1.95	2.00	1.95
Ti	0.03	0.03	0.03	0.01	0.02	0.02	0.02	0.02	0.02	0.02	0.00	0.00	0.00
Al	0.19	0.18	0.18	0.10	0.12	0.11	0.10	0.11	0.10	0.10	0.06	0.03	0.06
Cr	0.00	0.00	0.00	0.00	0.00	0.00	0.00	0.00	0.00	0.00	0.00	0.00	0.01
Fe^{3+}	0.09	0.07	0.07	0.00	0.02	0.03	0.01	0.03	0.02	0.01	0.04	0.00	0.00
Fe^{2+}	0.17	0.21	0.19	0.20	0.19	0.18	0.20	0.19	0.19	0.20	0.46	0.41	0.41
Mn	0.01	0.01	0.01	0.01	0.01	0.01	0.01	0.00	0.00	0.00	0.03	0.02	0.02
Mg	0.70	0.68	0.68	0.83	0.81	0.83	0.76	0.75	0.76	0.77	0.47	0.54	0.56
Ca	0.92	0.92	0.92	0.86	0.87	0.87	0.93	0.92	0.92	0.92	0.97	0.98	0.97
Na	0.04	0.04	0.05	0.04	0.04	0.04	0.04	0.05	0.04	0.04	0.01	0.01	0.02
K	0.00	0.00	0.00	0.00	0.00	0.00	0.00	0.00	0.00	0.00	0.00	0.00	0.00
Total	4.00	4.01	4.00	4.00	4.01	4.03	4.00	4.01	4.00	4.00	3.99	3.99	4.00
mg#	0.73	0.77	0.72	0.80	0.81	0.82	0.80	0.80	0.80	0.80	0.51	0.57	0.58
En	0.37	0.38	0.37	0.44	0.43	0.44	0.40	0.40	0.40	0.41	0.25	0.28	0.29
Fs	0.14	0.11	0.14	0.11	0.10	0.10	0.10	0.10	0.11	0.10	0.24	0.21	0.21
Wo	0.49	0.51	0.49	0.46	0.46	0.46	0.49	0.50	0.49	0.49	0.51	0.51	0.50
P(kbar)	12.07	12.46	12.77	17.21	19.87	18.7	17.29	19.77	18.24	17.14	8.87	7.00	9.56
T(°c)	1270	1271	1268	1402	1368	1398	1333	1346	1337	1338	1016	1038	1043
KD	0.31	0.31	0.31	0.33	0.32	0.33	0.32	0.32	0.32	0.32	0.29	0.29	0.29
Rock	Group 4								Potassic volcanics[a]		Intermediate volcanics		
Sample	kh-7	kh-7	kh-87	kh-87	k-40	k-40	k-40	k-40	GI5	GI5	v-kh-7	v-kh-87	v-kh-87
Location	Core	Core	Core	Core	Core	Rim	Core	Rim	Core	Rim	Core	Core	Rim
SiO_2	48.63	48.97	49.84	47.31	51.1	51.42	47.87	48.52	50.9	50.96	51.96	49.26	48.67
TiO_2	1.18	1.22	0.87	1.38	0.99	0.92	1.96	1.54	1.23	1.10	0.42	1.10	1.11
Al_2O_3	5.35	5.00	4.61	6.21	3.08	2.91	6.13	4.79	3.20	3.17	1.66	3.84	3.77
Cr_2O_3	0.02	0.01	0.02	0.00	0.00	0.00	0.00	0.00	0.01	0.00	0.01	0.00	0.00
FeOt	7.71	7.53	8.71	9.33	6.24	6.19	7.36	6.99	6.95	6.51	8.76	8.65	8.25
MnO	0.14	0.15	0.27	0.19	0.14	0.20	0.14	0.18	0.17	0.13	0.68	0.37	0.40
MgO	12.32	12.69	12.43	11.16	14.07	14.00	12.20	12.42	14.54	14.7	12.35	12.66	12.66
CaO	23.56	23.52	23.02	22.88	23.37	23.55	23.31	23.89	22.42	23.02	22.39	22.43	22.18
Na_2O	0.45	0.44	0.56	0.50	0.37	0.39	0.52	0.53	0.73	0.64	0.74	0.64	0.68
K_2O	0.00	0.00	0.01	0.00	0.00	0.00	0.01	0.00	0.02	0.06	0.00	0.00	0.01
Total	99.36	99.56	100.34	98.96	99.40	99.58	99.50	98.86	100.17	100.29	98.97	98.94	97.76
	Cations calculated on the basis of 6 oxygens												
Si	1.82	1.83	1.85	1.79	1.90	1.91	1.79	1.82	1.87	1.87	2.00	1.85	1.88
Ti	0.03	0.03	0.02	0.04	0.03	0.03	0.06	0.04	0.03	0.03	0.01	0.03	0.03
Al	0.24	0.22	0.20	0.28	0.14	0.13	0.27	0.21	0.14	0.14	0.07	0.17	0.16
Cr	0.00	0.00	0.00	0.00	0.00	0.00	0.00	0.00	0.00	0.00	0.00	0.00	0.00
Fe^{3+}	0.09	0.09	0.09	0.10	0.03	0.03	0.08	0.09	0.10	0.00	0.03	0.11	0.07
Fe^{2+}	0.15	0.15	0.18	0.19	0.16	0.16	0.15	0.13	0.11	0.20	0.24	0.17	0.18
Mn	0.00	0.01	0.01	0.01	0.00	0.00	0.00	0.00	0.01	0.00	0.02	0.01	0.01

Table 2 (continued)

Mg	0.69	0.71	0.69	0.63	0.78	0.78	0.68	0.70	0.80	0.80	0.70	0.71	0.73
Ca	0.95	0.94	0.92	0.93	0.93	0.94	0.93	0.96	0.88	0.91	0.91	0.90	0.90
Na	0.03	0.03	0.04	0.04	0.03	0.03	0.04	0.04	0.05	0.05	0.05	0.05	0.04
K	0.00	0.00	0.00	0.00	0.00	0.00	0.00	0.00	0.00	0.00	0.00	0.00	0.00
Total	4.00	4.01	4.00	4.00	4.00	4.00	4.00	4.00	4.00	4.00	4.03	4.00	4.00
mg#	0.74	0.83	0.72	0.68	0.83	0.83	0.82	0.85	0.87	0.80	0.72	0.81	0.73
En	0.36	0.39	0.37	0.34	0.41	0.40	0.38	0.37	0.44	0.42	0.37	0.40	0.38
Fs	0.14	0.08	0.14	0.16	0.10	0.11	0.10	0.12	0.06	0.10	0.15	0.10	0.14
Wo	0.50	0.52	0.49	0.50	0.50	0.49	0.52	0.51	0.50	0.48	0.48	0.50	0.48
P(kbar)	14.40	13.44	4.39	4.28	4.91	4.91	7.14	6.50	12.77	12.36	2.79	5.17	5.00
T(°c)	1152	1171	1101	1065	1214	1208	1171	1194	1171	1150	1110	1103	1095
KD	0.29	0.29							0.29	0.29		0.26	0.26

[a] Data for potassic and ultrapotassic volcanic rocks are from Ahmadzadeh et al. (2010)

field (Fig. 4b). It also has lower Mg# values (0.51–0.6) compared to those of clinopyroxenes from other clinopyroxenites. Clinopyroxenes in k-33 also displays lower MgO and Al_2O_3 and higher FeOt, Na_2O, and MnO contents (Table 2 and Electronic Appendix 2). We compared the chemical compositions of the clinopyroxene from the investigated pyroxenite xenoliths, with those of xenoliths from Spanish Central System (Al-augite series) (Orejana et al. 2006), mantle pyroxenites (Cr-diopside series) from NE Iran (Saadat and Stern 2012), and Alaskan-type massifs (Himmelberg and Loney 1995). The clinopyroxenes of the pyroxenites from the Spanish Central System have different compositions than those of Groups 1, 2, and 3 (Fig. 4b). They plot in the diopside field and closer to the Group 2 samples. However, the clinopyroxenes of Spanish pyroxenites differ from the latter in their lower CaO and higher Al_2O_3 contents. The clinopyroxenes of the pyroxenites from NE Iran also differ from those of Groups 1 to 4, due to higher MgO, SiO_2 and Cr_2O_3, and lower FeOt and Al_2O_3 contents. Finally, some clinopyroxenes from Alaskan-type pyroxenites display some similarities with those of Group 2, while some others are similar to those of Groups 1 and 4. However, the TiO_2 and Na_2O contents of clinopyroxenes from the investigated samples are higher than those of clinopyroxenes from the Alaskan samples. The clinopyroxenes from Alaskan-type clinopyroxenites have higher MgO and Al_2O_3 and lower FeOt and MnO contents than those of Group 3 sample.

Amphibole

Amphiboles occurring in Group 1 and Group 4 clinopyroxenite xenoliths both have a magnesio-hastingsite composition (Fig. 4d) with a Mg# varying from 0.58 to 0.69 (Table 3 and Electronic Appendix 3). According to the Si vs Na + Ca + K plot proposed by Sial et al. (1998), all the investigated volcanic rocks and xenoliths fall within the field of magmatic amphiboles (Fig. 4e). Their MgO, TiO_2, FeOt, CaO, Na_2O, K_2O, and Al_2O_3 contents are 10.16–12.51, 2.94–4.23, 11.87–15.63, 11.76–12.37, 2.07–2.48, 1.3–1.81 and 12.15–13.88 wt.%, respectively (Table 3 and Electronic Appendix 3). Similar to the xenoliths, the amphibole from intermediate volcanic rocks has a magnesio-hastingsite composition and a Mg# of 0.6. In Fig. 4d the location of amphiboles in Group 1 and 4 is similar to those of intermediate volcanic rocks. In comparison with xenoliths, amphiboles of intermediate volcanic rocks have slightly higher SiO_2 and MnO and lower Al_2O_3 contents (Table 3 and Electronic Appendix 3). In sample k-40 (Group 4), element concentrations do not show large variation from core to rim. There is no amphibole in potassic and ultrapotassic volcanic rocks as well as in Group 2 clinopyroxenite xenoliths. The composition of amphiboles of Alaskan-type clinopyroxenites is pargasitic and magnesio-hastingsitic. These amphiboles have higher CaO and Al_2O_3 and lower TiO_2 and Na_2O contents than those of the investigated samples from the present study.

Whole rock major and trace element chemistry

The major and trace element analyses of the xenoliths, intermediate volcanic rocks (host volcanic rocks) and potassic and ultrapotassic volcanic rocks are listed in Table 4 and Electronic Appendix 4. Most of the data plot in the alkali-rich field of the TAS diagram (Fig. 5a). Figure 5b illustrates the sample compositions in terms of K_2O vs Na_2O, according to Peccerillo and Taylor (1976). In this diagram, the intermediate volcanic rocks plot in the shoshonite and calk-alkaline fields, the potassic and ultrapotassic volcanic rocks plot in the high potassic and shoshonite fields, Groups 2 and 3 of clinopyroxenite xenoliths plot in the high potassic field, and Groups 1 and 4 of clinopyroxenite xenoliths plot near the boundary between shoshonite and calk-alkaline fields. The potassic and ultrapotassic volcanic rocks contain higher CaO, MgO, and TiO_2 contents than those of the intermediate rock but they are lower than those of the clinopyroxenite xenoliths (Table 4 and Electronic Appendix 4). The Group 3 clinopyroxenite

Table 3 Mineral chemical composition of amphiboles in clinopyroxenite xenoliths and volcanic rocks

Rock	Group 1			Group 4								Intermediate volcanics	
Sample	k-3	k-3	k-3	kh-87	kh-87	kh-87	K-40	K-40	kh-7	kh-7	kh-7	v-kh-7	v-kh-7
Location	Core	Core	Core	Core	Core	Core	Core	Rim	Core	Core	Core	Core	Core
SiO_2	40.31	40.30	39.31	39.41	40.11	39.20	40.14	40.52	40.03	39.49	39.82	41.61	41.10
TiO_2	2.96	3.08	3.59	3.10	3.03	3.14	4.23	4.08	2.94	3.19	3.22	3.03	3.06
Al_2O_3	12.15	12.68	13.14	13.88	13.54	13.62	12.79	12.42	12.94	13.03	13.45	11.14	11.16
Cr_2O_3	0.00	0.00	0.01	0.01	0.00	0.03	0.01	0.01	0.00	0.01	0.00	0.01	0.01
FeOt	12.39	12.41	13.02	13.14	12.63	13.45	11.92	11.87	14.18	15.63	14.63	15.02	15.33
MnO	0.14	0.13	0.17	0.20	0.18	0.19	0.07	0.17	0.21	0.19	0.17	0.31	0.31
MgO	12.44	12.25	11.54	11.72	11.59	11.72	12.25	12.51	10.93	10.16	10.75	11.14	10.98
CaO	11.94	11.84	11.87	12.17	11.97	11.95	12.37	12.11	11.91	12.00	12.09	11.68	11.59
Na_2O	2.39	2.37	2.25	2.07	2.14	2.14	2.08	2.19	2.29	2.35	2.35	2.18	2.25
K_2O	1.39	1.47	1.37	1.65	1.81	1.74	1.59	1.61	1.36	1.37	1.36	1.45	1.53
Total	96.11	96.53	96.27	97.35	97.00	97.18	97.45	97.49	96.79	97.42	97.84	97.57	97.32
	Cations calculated on the basis of 23 oxygens												
Si	6.11	6.09	5.97	5.91	6.05	5.91	6.00	6.05	6.07	6.00	5.99	6.28	6.23
Ti	0.34	0.35	0.41	0.35	0.34	0.36	0.48	0.46	0.34	0.37	0.37	0.34	0.35
Al (IV)	1.89	1.91	2.03	2.09	1.95	2.10	2.00	1.95	1.93	2.00	2.01	1.72	1.77
Al (VI)	0.29	0.34	0.33	0.37	0.46	0.32	0.25	0.24	0.39	0.34	0.38	0.26	0.22
Cr	0.00	0.00	0.00	0.00	0.00	0.00	0.00	0.00	0.00	0.00	0.00	0.00	0.00
Fe^{3+}	0.29	0.27	0.29	0.46	0.25	0.51	0.00	0.00	0.26	0.29	0.27	0.25	0.31
Fe^{2+}	1.29	1.30	1.36	1.19	1.34	1.19	1.49	1.48	1.54	1.70	1.57	1.64	1.63
Mn	0.02	0.02	0.02	0.03	0.02	0.02	0.01	0.02	0.03	0.02	0.02	0.04	0.04
Mg	2.81	2.76	2.61	2.62	2.61	2.63	2.73	2.79	2.47	2.30	2.41	2.51	2.48
Ca	1.94	1.92	1.93	1.96	1.94	1.93	1.98	1.94	1.94	1.95	1.95	1.89	1.88
Na	0.70	0.70	0.66	0.60	0.63	0.63	0.60	0.63	0.67	0.69	0.69	0.64	0.66
K	0.00	0.00	0.00	0.00	0.00	0.00	0.30	0.31	0.00	0.00	0.00	0.00	0.00
Total	15.68	15.66	15.61	15.58	15.59	15.60	15.84	15.87	15.64	15.66	15.66	15.57	15.57
Mg≠	0.69	0.68	0.66	0.69	0.66	0.69	0.65	0.65	0.62	0.58	0.61	0.60	0.60

xenolith k-33 has higher K_2O and Al_2O_3 and lower CaO contents, compared to other groups of clinopyroxenite xenoliths.

The multi element diagram of the investigated xenoliths and volcanic rocks normalized to primitive mantle values are presented in Figs. 6 and 7. As shown in Fig. 6, the trace element contents of the volcanic rocks indicate a noticeable enrichment in large-ion lithophile elements (LILE) such as Ba, U, K, and LREE over HFSE (Ta, Nb, Ti, Zr, Hf,) and HREE. In addition, volcanic rocks display negative anomalies in elements such as Ta, Hf, Zr, P, Nb, and Ti (Fig. 6a, c). The negative Ta and Nb anomaly is similar to that of magmatic rocks from active continental subduction margins (Gill 1981; Kelemen et al. 1992; Gertisser and Keller 2000; Rudnick and Gao 2003). Contents of REE and some other incompatible elements such as Ba, U, Th, and Rb in potassic and ultrapotassic volcanic rocks are higher than those of intermediate volcanic rocks. The potassic and ultrapotassic volcanic rocks also display a higher negative Eu anomaly compared to the intermediate volcanic rocks.

Most samples from Groups 2 and 4 are characterized by a distinct enrichment in Ba, U, Pb, Sm, P, Nd, La, Ce and K, and by a depletion in Ta and Ti (Fig. 7c, g). In Group 1, contents of incompatible elements are lower than those in Groups 2 and 4. Group 1 displays positive anomalies of Ti, Sm, Pb and Nd and negative ones of P, K and Th (Fig. 7a).

Group 3 (k-33 sample), when compared to other groups, has a higher K content, probably related to the high modal abundance of biotite (40%) in this sample. The contents of HFSE (Ta, Nb, Ti, Zr and Hf) in Group 3 are lower than those of the other xenoliths and, unlike to Group 2 and 4, a positive Ti anomaly and a negative anomaly of La, Ce and P is observed for this group (Fig. 7e). All volcanic rocks and xenolith samples display a positive Pb anomaly but they are higher in the volcanic rocks compared to the xenoliths.

Rare earth element diagrams normalized to chondrite values (normalizing value from Boynton 1984) are presented in Fig. 7b–h. Three different types of patterns are distinguished for the xenoliths. Groups 2 and 4, which comprise

Table 4 Whole-rock major and trace element data for xenoliths and volcanic rocks from northwestern Marand. Fe_2O_3 as total Fe_2O_3. Major elements in wt.%, trace elements and REE in ppm

Rock	Group 1	Group 2			Group 3	Group 4		Intermediate volcanic rocks					Potassic volcanics[a]	
Sample	K-3	Kh-14	Kh-64	Kh-62	K-33	Kh-7	Kh-93	V-Kh-65	Kh-87	V-Kh-52	V-K-20	V-Kh-93	DL13	GL5
SiO_2	42.41	43.17	42.83	43.11	45.32	36.33	34.56	59.55	52.52	58.74	64.85	52.70	48.90	50.00
TiO_2	2.14	2.04	2.05	1.99	1.22	2.72	2.61	0.80	1.11	0.82	0.64	1.15	1.23	1.22
Al_2O_3	5.72	5.75	5.15	5.79	14.8	7.80	6.86	15.72	17.36	16.00	17.15	17.54	13.25	13.05
Fe_2O_3	17.76	12.81	13.99	11.69	12.76	20.24	24.43	5.37	8.14	5.33	5.15	8.50	7.87	8.19
MnO	0.22	0.21	0.17	0.15	0.23	0.21	0.33	0.09	0.16	0.09	0.05	0.19	0.14	0.13
MgO	11.16	13.12	12.53	12.78	9.30	8.85	7.57	3.56	2.53	3.42	0.96	2.79	5.92	6.58
CaO	19.02	17.11	18.40	18.63	6.48	17.37	17.89	5.80	7.68	5.78	3.69	7.73	9.37	9.38
Na_2O	0.82	0.89	0.67	0.58	1.73	1.38	1.07	4.97	4.50	4.92	4.10	4.98	1.34	2.35
K_2O	0.25	2.53	1.75	2.06	4.74	0.67	0.30	2.94	2.85	3.05	3.48	2.58	6.46	5.55
P_2O_5	0.25	2.12	2.46	2.59	0.15	2.87	2.86	0.40	0.58	0.39	0.31	0.62	1.14	1.20
LOI	0.27	1.66	0.89	0.63	1.99	0.48	1.19	0.54	2.33	1.55	0.82	2.56	4.37	2.51
Total	100.01	100.41	100.01	100.01	98.72	98.91	99.66	99.74	99.77	100.09	101.19	101.33	99.99	100.16
Sr	210	225	390	470	92	443	405	821	1247	1002	673	867	2680	1110
Ba	90	2261	1698	4116	360	250	129	909	872	834	1231	879	2620	2470
V	529	270	338	263	230	596	611	93	184	97	109	202	280	262
Cr	47	477	334	320	438	29	34	138	20	135	11	5	160	210
Co	73	60	62	59	45	81	56	33	26	27	28	27	36	37
Ni	68	167	96	96	206	67	18	67	16	67	7	8	48	49
Y	22	37	35	30	19	35	52	14	34	15	13	32	24	25
Zr	98	65	84	87	40	152	153	157	241	162	83	216	344	324
Nb	5.0	16.8	8.4	10.6	6.9	8.6	7.1	22.7	19.6	23.2	13.5	16.6	53.3	47.5
Mo	0.5	0.8	0.8	0.7	3.7	1.2	0.8	0.8	2.5	1.4	2.3	1.0	2.0	4.0
La	7.7	77.9	62.3	34.5	2.4	42.7	38.1	29.9	18.9	42.9	24.8	15.9	66.0	61.7
Ce	24.9	163.9	142.8	73.8	6.6	106.1	85.8	69.0	47.1	89.5	53.8	34.3	138.5	128.0
Pr	3.8	21.6	19.7	10.8	1.0	14.1	12.0	7.0	5.1	10.4	5.5	4.3	16.8	15.6
Nd	17.7	91.2	85.4	48.3	5.1	66.1	54.9	25.7	21.2	38.4	19.4	16.8	67.0	62.9
Sm	6.2	17.1	16.7	9.3	1.6	13.9	11.5	4.4	4.2	6.7	3.5	3.5	12.8	12.3
Eu	1.8	3.4	3.3	1.8	0.4	3.8	2.8	1.1	1.1	1.6	1.0	0.9	2.8	2.8
Gd	6.0	12.1	12.1	7.1	2.1	11.6	10.4	3.1	3.6	4.7	2.8	3.1	10.6	10.5
Tb	0.8	1.4	1.4	0.8	0.4	1.6	1.4	0.4	0.5	0.6	0.4	0.4	1.3	1.3
Dy	4.4	6.7	6.7	3.5	2.4	7.6	6.9	2.1	2.5	3.2	2.3	2.3	5.9	5.8
Ho	0.8	1.2	1.1	0.6	0.5	1.3	1.2	0.4	0.5	0.6	0.4	0.4	1.0	1.0
Er	2.0	2.9	2.5	1.2	1.5	3.6	3.1	1.0	1.3	1.5	1.2	1.2	2.7	2.7
Yb	1.5	2.0	1.5	0.7	1.3	2.2	2.1	0.8	1.1	1.4	1.1	1.0	2.0	1.9
Hf	2.0	1.6	2.3	1.2	0.9	2.4	1.8	4.4	4.7	4.7	3.1	4.5	9.1	8.0
W	92.1	21.4	22.6	37.0	18.8	17.8	31.5	70.7	29.8	64.2	121.6	44.7	7.0	9.0
Th	0.2	3.4	3.3	1.2	0.1	4.3	2.4	10.9	2.3	21.2	8.1	1.3	32.8	29.7
U	0.2	1.5	1.2	1.0	0.3	1.8	3.3	6.1	5.5	6.8	3.5	4.2	8.2	9.7
Cu	15.7	50.1	36.1	48.9	25.5	12.5	78.8	175.1	79.6	40.5	18.7	44.7	133.1	90.2
Zn	113.0	123.4	85.4	65.2	265.1	130.8	160.4	46.4	86.3	50.8	62.8	89.8	118.3	125.1
Ga	15.9	11.5	9.2	8.6	13.9	22.5	20.4	16.9	18.4	18.4	18.6	17.8	20.7	19.8
Rb	2.6	74.2	48.2	45.1	42.9	11.9	10.9	38.9	10.1	46.5	67.2	10.3	187.1	170.2
Cs	0.2	3.1	2.1	1.9	4.0	0.8	1.5	0.6	0.6	2.2	9.1	4.1	8.7	10.0
Ta	0.2	0.4	0.3	0.5	0.4	0.3	0.3	1.5	0.5	1.6	1.0	0.6	3.0	2.5
Pb	4.3	3.2	3.1	2.2	7.7	12.8	13.6	15.2	57.6	15.6	23.9	26.0	35.0	57.0
Ba/Nb	18	134	203	390	52	29	18	40	45	36	91	53	49	52

Table 4 (continued)

Rock	Group 1	Group 2			Group 3	Group 4		Intermediate volcanic rocks					Potassic volcanics[a]	
Sample	K-3	Kh-14	Kh-64	Kh-62	K-33	Kh-7	Kh-93	V-Kh-65	Kh-87	V-Kh-52	V-K-20	V-Kh-93	DL13	GL5
Ba/Ta	450	5519	6291	8949	859	929	391	627	1677	512	1245	1391	873	988
Nb/La	0.7	0.2	0.1	0.3	2.9	0.2	0.2	0.8	1.0	0.5	0.6	1.0	0.8	0.8
Ce/Pb	5.7	52.0	45.5	33.5	0.9	8.3	6.3	4.6	0.8	5.7	2.3	1.3	4.0	2.3

[a] Data for potassic and ultrapotassic volcanic rocks are from Ahmadzadeh et al. (2010)

the majority of clinopyroxenite xenoliths, display similar REE patterns as the volcanic rocks and, similarly to the latter, are characterized by LREE enrichment over HREE (Fig. 7b, h). The $(Cr/Yb)_N$ ratios of the intermediate volcanic rocks, potassic and ultrapotassic volcanic rocks, and Groups 2 and 4 clinopyroxenite xenoliths are 8.4–21.9, 15.71–17.55, and 10.0–26.9, respectively (Table 4 and Electronic Appendix 3). The REE pattern shape for Group 1 is convex-upward indicating an enrichment in MREE over LREE and HREE (Fig. 7b). Moreover, Group 3 patterns show a relatively flat slope of $(Ce/Yb)_N = 1.36$. All groups, except Group 1, are characterized by negative Eu anomalies (Fig. 7b–h). The REE contents, Eu anomalies, and REE patterns of samples from Groups 4 and 2 are similar to those of intermediate volcanic rocks and potassic and ultrapotassic volcanic rocks, respectively.

The comparison of the whole rock analyses of clinopyroxenites from the present study with those of Alaskan-type rocks (Himmelberg and Loney 1995) reveals significant differences. For instance, the Kane Peak clinopyroxenites have higher SiO_2 and MgO and lower P_2O_5, Na_2O, K_2O, TiO_2, Al_2O_3, and FeOt contents than those of the investigated clinopyroxenites. Moreover, clinopyroxenites from Port Snettisham have higher FeOt and lower SiO_2 and P_2O_5 contents than those of the investigated clinopyroxenites. Furthermore the LREE and MREE contents of Group 2 and Group 4 clinopyroxenites are higher than those of Alaskan-type clinopyroxenites, while only the MREE content of Group 1 clinopyroxenite is higher than that of Alaskan-type clinopyroxenites. On the other hand the REE content of Group 3 clinopyroxenites is similar to that of Alaskan-type clinopyroxenites. Finally, the incompatible trace element contents such as those of Ba, Th, and U of the investigated samples are higher than those of Alaskan-type samples, while their compatible trace element contents such as those of Ni and Cr are lower.

Whole-rock Sr–Nd isotopes

The Sr and Nd isotopic data are presented in Table 5. The $^{87}Sr/^{86}Sr$ and $^{143}Nd/^{144}Nd$ of pyroxenite xenoliths (kh-62, kh-64 and kh-14 samples) vary from 0.706420 to 0.707026 and 0.512482 to 0.512561 (εNd: from −2.81 to −1.98), respectively. Figure 8 shows that the investigated samples plot within the upper crust and EMI fields. The ratios of $^{143}Nd/^{144}Nd$ and $^{87}Sr/^{86}Sr$ in the volcanic host rock of the xenoliths (v-kh-52) are 0.512561 and 0.709545 (εNd:-1.27), respectively, and plot near the upper crust field. The exact age of formation of clinopyroxenite xenoliths is not known. As mentioned in the geological setting section, the upper Miocene deposits are covered by the host volcanic rocks, and therefore it appears that the relative age of this volcanic series is younger than upper Miocene. However, based on the relative age of host volcanic rocks, we corrected the isotopic composition of the rocks to 5 million years. The ratios of $^{143}Nd/^{144}Nd$ and $^{87}Sr/^{86}Sr$ in host volcanic rocks of NE Iran are 0.512735–0512738 and 0.705013–0.705250, respectively and the ratios of $^{143}Nd/^{144}Nd$ and $^{87}Sr/^{86}Sr$ in pyroxenite xenolith of NE Iran are 0.512798 and 0.704593, respectively

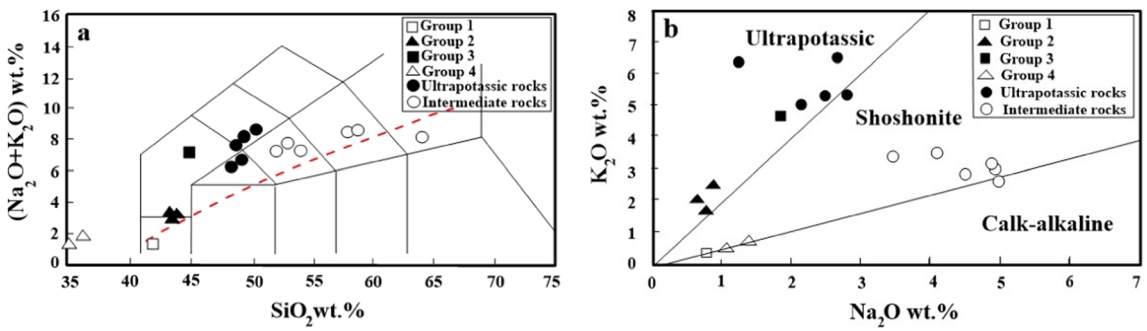

Fig. 5 Clinopyroxenite xenoliths and volcanic rocks (**a**) plotted in the TAS diagram (Le Bas et al. 1986). Dashed line separates subalkaline from alkaline rocks. Most of the data plot in the alkaline field. **b** plotted in the Na_2O vs. K_2O diagram

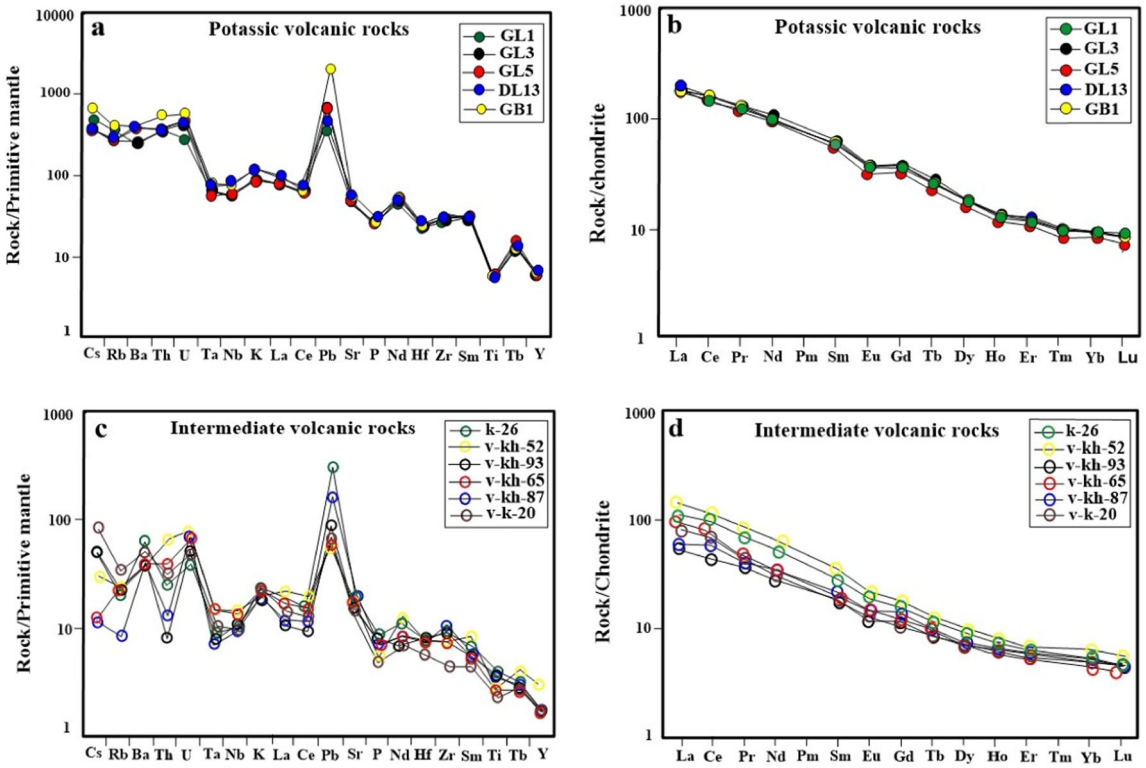

Fig. 6 Chondrite normalized REE patterns and primitive mantle normalized spidergrams of the volcanic rocks. Chondrite and primitive mantle values are from Boynton (1984) and McDonough et al. (1992), respectively (except for P which is from Wood et al. 1979)

(Saadat and Stern 2012). As illustrated in Fig. 8 the samples from NE Iran are not similar to those from NW Marand.

Discussion

P-T conditions

Due to the lack of minerals such as garnet, olivine, and orthopyroxene in the investigated xenoliths and volcanic rocks, clinopyroxene was used for thermobarometry according to the method proposed by Putirka (2008). Eqs. 32b and 32c of Putirka (2008) have been used for P estimates. Eq. 32b is based on clinopyroxene composition only and eq. 32c is based on the partitioning of Al between clinopyroxene and liquid. Most of the investigated samples were analyzed both for whole rock and clinopyroxene, therefore we used Eq. 32c in those cases, but only clinopyroxenes were analyzed for samples k-40, kh-87 and v-kh-7, therefore we used eq. 32b for them. Eq. 32d based on clinopyroxene composition only is also used for thermometry because as mentioned by Putirka (2008) this equation is a new and more precise thermometer. All those eqs. (32b, 32c and 32d) appear in the section "Clinopyroxene and clinopyroxene-liquid thermobarometers" of the original paper of Putirka (2008; Page 79). Formation temperature of clinopyroxenes in Groups 1 to 4 of xenoliths, intermediate volcanic rocks and potassic and ultrapotassic volcanic rocks were estimated at 1245–1280, 1310–1400, 1015–1040, 1065–1225, 1070–1225 and 1045–1170 °C, respectively (Table 2 and Electronic Appendix 2). According to Putirka (2008), if K_D (the partition coefficient of Fe-Mg between clinopyroxene and melt) is within 0.28 ± 0.08, then the clinopyroxene can be assumed to be in equilibrium with the melt. Since the K_D of the investigated volcanic rocks (0.25–0.29) and pyroxenite xenoliths (0.28–0.32) fall within this range, the chemical composition of their clinopyroxene and whole rock is suitable to be used for barometry. The estimated formation pressures for clinopyroxene of intermediate volcanic rocks (v-kh-87) and potassic, and ultrapotassic volcanic rocks are 4–7, and 9–12.5 kbar, respectively. The crystallization of potassic and ultrapotassic volcanic rocks therefore occurred at greater depth than that of the intermediate volcanic rocks. The formation pressure for clinopyroxene of Groups 1 to 4 (kh-7 sample) clinopyroxenite xenoliths are 11.5–13, 17–21, 7–9.5 and 12–14 kbar, respectively, using Eq. 32c. The formation pressure of clinopyroxene of the two other Group 4 (kh-87 and k-40 samples) clinopyroxenite xenoliths as well as that of the intermediate volcanic rock (v-kh-7 sample) are 4–7 and 0.5–3 kbar, respectively, using Eq. 32b (Table 2 and Electronic Appendix 2). The formation pressure and temperature for the core and the rim of clinopyroxene in volcanic rocks and pyroxenite xenoliths (samples kh-64 and k-40) do not show significant difference. Indeed the formation pressure for the rim

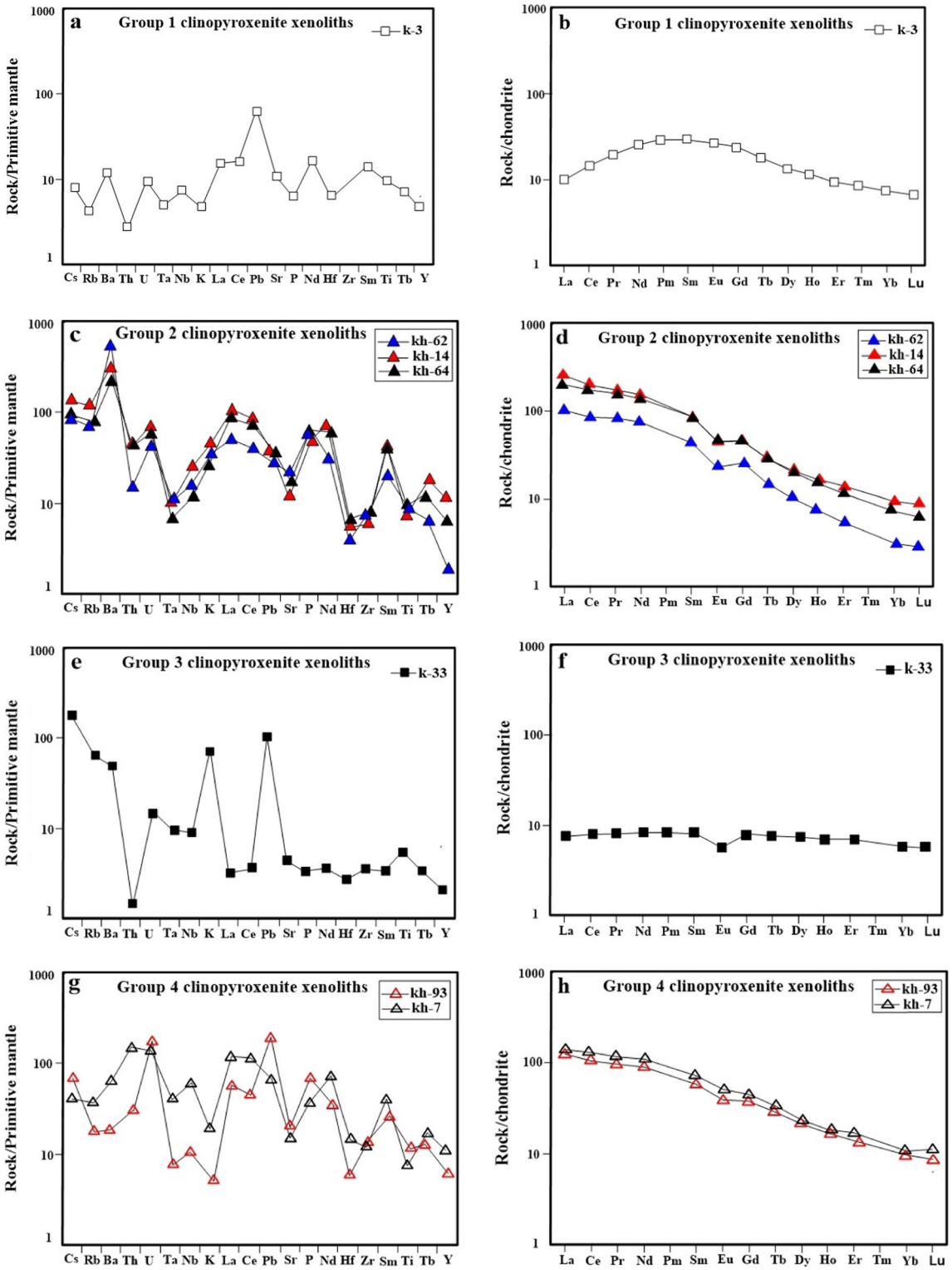

Fig. 7 Chondrite normalized REE patterns and primitive mantle normalized spidergrams of clinopyroxenite xenoliths. Chondrite and primitive mantle values are from Boynton (1984) and McDonough et al. (1992), respectively (except for P which is from Wood et al. 1979)

are slightly less than for the core while the formation temperature for core and rim are approximatively equal. The almost homogeneous composition of clinopyroxenes of Group 2 and Group 4 xenoliths and volcanic rocks indicates slow crystallization and equilibrium processes of clinopyroxenes with the melt.

The crystallization depth of Group 2 clinopyroxenites is therefore estimated at about 50–60 km while for Group 1, 3

Table 5 Sr and Nd isotopic (Whole-rock) composition of xenoliths and a volcanic rock from NW Marand area

	Sample	$^{87}Sr/^{86}Sr$	2σ	$^{143}Nd/^{144}Nd$	2σ	εNd
Group 2 clinopyroxenite xenoliths	kh-62	0.707026	0.000003	0.512525	0.000003	-1.98
	kh-64	0.706825	0.000003	0.512482	0.000002	-2.81
	kh-14	0.706420	0.000002	0.512501	0.000002	-2.45
Intermediate volcanic rock	v-kh-52	0.709545	0.000002	0.512561	0.000002	-1.27

and 4 it ranges from 35 to 39, 20 to 30 and 12 to 40 km, respectively. Since the crustal thickness in the area is about 40–45 km as determined by geophysical studies (Dehghan and Makris 1984), it seems that samples of Group 2 formed within the upper mantle just below the crust while samples of Groups 1, 3 and 4 formed within the crust. The source of volcanic rocks was of course located at a depth of more than 50 km in order to be able to collect and carry the xenoliths to the Earth surface. Clinopyroxene minerals in sample k-40 formed at two different depths, some of them crystallized at a depth of 20 to 22 km while others formed at a depth of approximatively 15–16 km.

Clinopyroxenes of Group 2 xenoliths are characterized by high temperatures. Putirca et al. (1996) explained such kind of high temperatures by a re-heating event of rocks within the crust and/or the mantle due to a hot plume effect. These authors indeed estimated formation temperatures of clinopyroxene phenocrysts in mafic igneous rocks from Mauna Kea, Hawaii ranging from 1100 to 1470 °C (with a corresponding pressures of 8 to 30 kbar) and attributed these high formation temperatures to a hot plume beneath the area. Because the volume of volcanic rocks in our case is much lower than that of the above mentioned study, and because no high-temperature minerals were previously reported from adjacent areas, the high formation temperature of clinopyroxenes from Group 2 xenoliths cannot be attributed to a hot plume activity. Rather, it is more logical to attribute the local heating evidenced by Group 2 to a younger magmatic activity connected to magmatic intrusions within the lithosphere.

The nature of mantle sources in the northwest of Marand

The chemistry of the investigated volcanic rocks indicates that most of them have a shoshonitic and ultrapotassic affinity (Fig. 5b), and are enriched in incompatible trace elements such as Ba, Pb, U, K, and Sr. Moreover these rocks have high LILE/HFSE ratios and are relatively depleted in Ta, Nb, and Ti (Fig. 6a, c). All these features are characteristic of subduction magmatism (i.e. Barth et al. 2000; Patchett and Chase 2002; Green 2006). Furthermore Ba/Ta and Ba/Nb ratios higher than 450 and 28, respectively also evidence subduction magmatism (Fitton et al. 1991). In our volcanic rocks, Ba/Ta and Ba/Nb ratios range from 512 to 1966 and from 36 to 103 respectively, evidencing the influence of subduction components in their evolution. The Sr and Nd isotopic ratios of intermediate volcanic rocks evidence the occurrence of an enriched component in their mantle source (Table 5).

Considering the great thickness of the continental crust below the investigated area (40 to 45 km) and the crystallization of most of the clinopyroxenes at relatively low pressures (4 to 12.5 kbar) within the crust, we infer that crustal contamination may have also occurred. Nb/La < 1 is a good indicator of crust-contaminated magma (Kieffer et al. 2004), and since this ratio is indeed <1 for the majority of the investigated volcanic rocks (Table 4 and Electronic Appendix 4), this

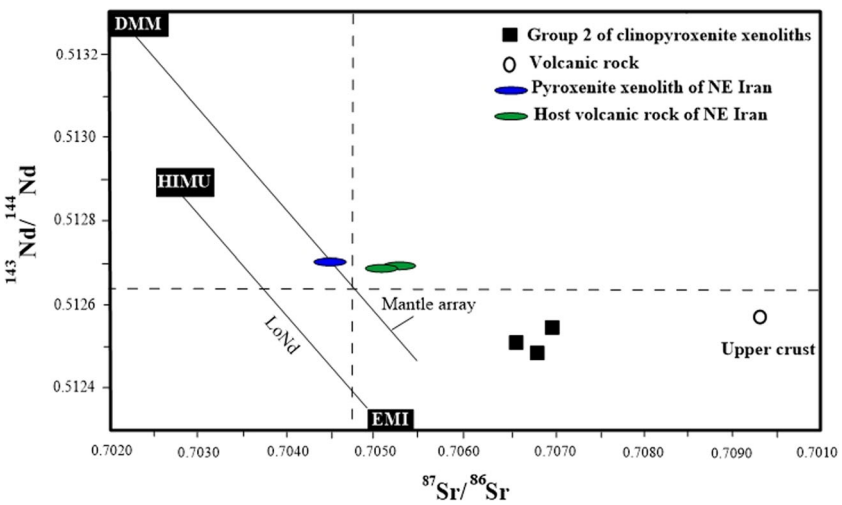

Fig. 8 $^{143}Nd/^{144}Nd$ vs. $^{87}Sr/^{86}Sr$ diagram for the whole rock of samples kh-62, kh-64, kh-14 and v- kh-52. The fields of DMM, HIMU, EM1, upper crust are from Zindler and Hart (1986). LoNd array is from Hart et al. (1986). NE Iran data are from Saadat and Stern (2012)

points to crustal contamination. Ce/Pb in the investigated volcanic rocks ranges from 0.55 to 5.73, i.e. it is considerably lower than in mid-ocean ridge basalts and arc basalts that are 47 and 27, respectively (Hofmann et al. 1986). This also strengthens the hypothesis that some crustal materials may have occurred within the source (Yang et al. 2005). According to Hess (1989) an initial magma generated by the partial melting of the peridotitic upper mantle typically contains around 400 ppm Ni and 600 ppm Cr. The Cr content in the investigated intermediate and potassic-ultrapotassic volcanic rocks ranges from 5 to 139 and from 160 to 280 ppm, respectively, while their Ni content ranges from 7 to 80 and 39 to 60 ppm, respectively. These low contents of Cr and Ni might be attributed to the fractionation of olivine and clinopyroxene from the initial magma. The lack of olivine and the low modal content of clinopyroxene of the volcanic rocks, is in agreement with this observation.

To constrain the source and the melting rate of the investigated volcanic rocks, the La/Yb vs. Yb diagram was used (Fig. 9). In this diagram the intermediate volcanic rocks plot near the garnet lherzolite melting curve, while the potassic and ultrapotassic volcanic rocks occur above that curve and to the right of the spinel lherzolite melting curve. On the other hand the potassic and ultrapotassic volcanic rocks plot close to the mixing line involving mixing of 0.5% melt fraction from garnet-facies source with 5% melt fraction from spinel-facies source (Fig. 9). As shown in Fig. 9, the intermediate volcanic rocks could have been formed by 2 to 5% of melting of a spinel lherzolite source. According to Rollinson (1993), the high LREE contents compared to HREE associated with low Yb and Y contents and high La/Yb ratios, can be explained with the equilibrium between a melt and garnet and/or hornblende (as a residual phase in the source). The positive K anomaly in the spider diagram of volcanic rocks (Figs. 6a, c) is probably related to the occurrence of K-bearing minerals such as phlogopite in the magma source. The silica-under saturated lavas in the Islamic peninsula (near the study area) with an age of 8–11 Ma (Moradian et al. 1997; Pang et al. 2013; Shafaii Moghadam et al. 2013) in terms of petrographic characteristics (i.e., the presence of clinopyroxene, apatite, phlogopite and leucite minerals and texture) are similar to the potassic and ultrapotassic volcanic rocks of our study area. They show similar to the volcanic rocks of northwestern Marand evidence of extensive metasomatism.

Generation of the volcanic rocks

The origin of intraplate alkaline rocks both in oceanic and continental settings is mainly related to mantle plume activity (Willson 1989). Typically, the plume-related magmatism results from the melting of an enormous volume of rocks and leads to huge eruptions (Saunders et al. 1991). In this regard, it is observed that alkaline rocks from northwestern Marand have a limited volume and geochemical characteristics such as Nb, Ta, and Ti depletion which are inconsistent with mantle plumes. Kheirkhah et al. (2009) linked the subduction-related magmatism of the Urumieh-Dokhtar magmatic belt to the failure of the subducted plate. As previously mentioned, the Neotethys oceanic plate was subducted beneath the Iranian continental crust during Middle Cretaceous (Ghasemi and Talbot 2006). The subduction of this plate led to metasomatism of the mantle wedge located above the subducting plate. According to Kheirkhah et al. (2009), the subduction angle of the subducting oceanic plate increased and that plate was torn apart in a slab break-off process leading to the formation of a slab window. Based on this model, the uplift of hot asthenosphere through the window lead to the heating and melting of the metasomatised lithospheric mantle. As mentioned earlier,

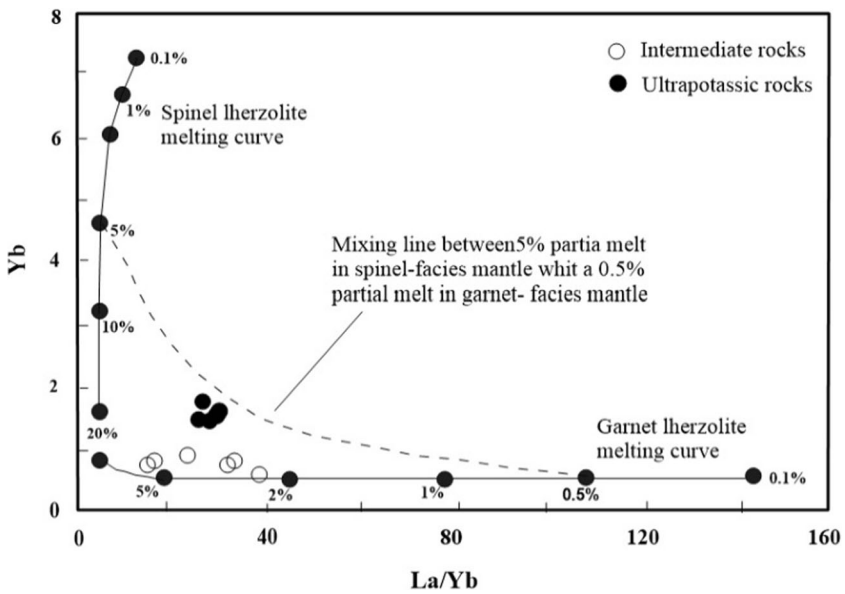

Fig. 9 Plot of La/Yb vs. Yb for the samples from northwestern Marand. Melt curves were calculated using the non-modal batch melting equations of Baker et al. (1997)

alkaline rocks are spatially limited to the northwest of Marand and only occur between North Tabriz, South Divan Daghi and Gharagoz Faults. It seems that the occurrence of a tensional regime along this complicated fault system, especially the movement to south of the Divan Daghi, Gharagoz and North Tabriz Faults, controlled the eruption of those magmas in the northwest of Marand.

Cumulate clinopyroxenite xenoliths

The xenolith-hosting volcanic rocks from NW Marand, unlike those from NE Iran (Saadat and Stern 2012), differ from ocean island basalts (OIB). Mantle pyroxenite xenoliths from NE Iran exhibit granular textures and unlike the pyroxenite xenoliths from NW Marand contain spinel and orthopyroxene. The chemical composition of clinopyroxene of pyroxenite xenoliths from the northwest of Marand differs from that of the clinopyroxene of clinopyroxenite xenoliths (Al-augite series) occurring in alkaline lamprophyres from Spanish Central System (Orejana et al. 2006) which sometimes contain spinel and orthopyroxene, never observed in the pyroxenites from the present study.

In terms of petrographic characteristics (i.e., the occurrence of clinopyroxene, amphibole, and phlogopite, cumulate texture) and chemical composition of clinopyroxenes, the investigated clinopyroxenites are similar to those of Alaskan-type massifs (Himmelberg and Loney 1995). However, they differ from the latter in terms of whole rock major and trace elements concentrations and composition of mica and amphibole.

The lower value of Al^{VI} of micas from xenoliths and volcanic rocks is main evidence for their magmatic origin (Nachit et al. 2005). The Ti content of mica is a function of temperature, pressure, and oxygen fugacity (Henry 1981; Arima and Edgar 1981). The differences in the Ti concentrations of micas of the investigated xenoliths suggest that they were formed at different temperature, pressure, and oxygen fugacity conditions.

Group 1 sample k-3 does not indicate a clear enrichment in incompatible elements except for Pb (Fig. 7a). Its negative K anomaly and lower Ba content compared to xenoliths of Group 2 and 4 can be explained with the lack of phlogopite, while the negative P and Ce anomalies are related to the low modal content of apatite. The LREE and HREE contents in k-3 are lower and similar to those of pyroxenites of Group 2 and 4 (Fig. 7). The MREE enrichment compared to LREE and HREE, the positive Ti anomaly and the lack of a negative Eu anomaly in this sample, are related to the modal abundance of amphibole (25%). The chemical composition of clinopyroxene and amphibole as well as the Ni (80 ppm) and Cr (39 ppm) whole rock contents of this group of clinopyroxenite display similarities with those of the intermediate volcanic rocks. The convex-upward REE pattern normalized to chondrite values is in agreement with a fractional differentiation process of pyroxene from a melt (e.g. McDonough and Frey 1989; Ho et al. 2000). That characteristic together with the low content of incompatible elements in Group 1 clinopyroxenite, points to an origin by mineral segregation from a melt within the crust. This is further supported by cumulate texture of this rock.

Group 2 pyroxenite xenoliths are the most abundant. Their trace element patterns normalized to chondrite values evidence a LREE enrichment over HREE, similar to those of the potassic and utrapotassic volcanic rocks (Fig. 7d). These xenoliths are relatively rich in Ba, U and Pb and relatively depleted in Ta and Ti (Fig. 7c). As shown in Fig. 7c, Group 2 clinopyroxenite xenoliths have negative anomalies in Th, Zr, Hf and Nb and positive anomalies in K and Ba, in agreement with an accumulation process of clinopyroxene and phlogopite. The positive anomaly of P and Ce is associated with the occurrence of apatite (Fig. 7c). As mentioned in the petrography section, small phlogopite and apatite crystals occur as inclusions in clinopyroxene indicating that they crystallized before the latter. The Sr and Nd isotopic ratios of the host volcanic rocks (v-kh-52) and Group 2 clinopyroxenite xenoliths evidence enrichment of their magmatic source. Continental crust is characterized by low Nd and high Sr isotopic ratios, whereas the upper mantle displays high Nd and low Sr isotopic ratios (Best and Christiansen 2001) and therefore any continental crust contamination process will increase the $^{87}Sr/^{86}Sr$ ratio and reduce the $^{143}Nd/^{144}Nd$ ratio (Koohestani et al. 2013). The higher $^{87}Sr/^{86}Sr$ ratio (0.709564) of the intermediate volcanic rock compared to Group 2 xenoliths (0.706555–0.707065), and the $^{143}Nd/^{144}Nd$ ratios seem to indicate that the origin of their enrichment is different (Table 5). The contents of compatible elements such as Ni (96–167 ppm) and Cr (320–477 ppm) in the whole rock of Group 2 are similar to those of the potassic and ultrapotassic volcanic rocks. Many previous studies have described similar cumulative pyroxenites (Porreca et al. 2006; Gonzaga et al. 2010; Zhang et al. 2010; Medaris et al. 2013).

Group 3 is high in some incompatible elements such as Rb, Ba, K, U and Pb and depleted in Ta and Nb. (Fig. 7e). The REE contents in this group are lower than in the other groups and in the volcanic rocks (Table 4 and Electronic Appendix 4). In addition, the REE patterns normalized to chondrite values have a flat slope, which is very different from the LREE enriched Groups 1, 2 and 4 xenoliths (Fig. 7f). Clinopyroxenes in this group have lower MgO, TiO_2 and Al_2O_3 contents and higher FeOt, Na_2O, and MnO contents compared to clinopyroxenes from other groups of xenoliths (Table 2 and Electronic Appendix 2). The Ti content in clinopyroxene is indicative of the degree of depletion of the mantle source of its parental melt (Pearce and Norry 1976). Low Ti in clinopyroxenes from Group 3 compared to the other groups could therefore indicate that the source of this group has experienced more depletion

and partial melting. Biotite crystallization and enrichment in some trace elements might be attributed to the presence of K-rich fluids. The positive anomalies of K, Rb, and Ba shown in Fig. 7e are related to the modal abundance of biotite (40%). The negative anomalies of P and Ce are instead related to the lack of apatite.

The REE patterns of Group 4 are similar to those of the intermediate volcanic rocks (Fig. 7h). The samples of this group are on the other hand different from the Group 2 samples in terms of crystal size, depth of crystallization, their Cr and Ni whole rock contents and the chemical composition of clinopyroxenes. The Ni (19–68 ppm) and Cr (29–34 ppm) contents in this group are lower than those of Group 2 xenoliths, and similar to those of the intermediate volcanic rocks (Table 4 and Electronic Appendix 4). These samples of Group 4, similar to those of Group 2, display negative anomalies in Th, Zr, Hf and Nb and positive anomalies in Ba, in agreement with an accumulation process of clinopyroxene, amphibole and phlogopite. K, Ba and Rb contents in the Group 4 are lower than those of the Group 2 samples, due to its lower modal content of phlogopite. The positive anomaly of P and Ce in this group is related to the occurrence of apatite (Fig. 7g). The high FeO_t whole rock content in this group is related to the relatively high modal abundance of opaque minerals. The occurrence of small inclusions of opaque minerals, phlogopite and apatite within clinopyroxene implies that these minerals crystallized before the host clinopyroxene. The variation in major elements of clinopyroxene minerals observed in Group 4 sample k-40 suggests that a first stage of crystallization of opaques and clinopyroxene at relatively great depth (20 to 22 km) modified the composition of the remaining magma. From the latter the rest of the clinopyroxenes crystallized at shallower depths (15–16 km).

Conclusions

The volcanic province in NW Marand area is limited by the Gharagoz and Divan Daghi Faults to the north and by the Mishou, Tabriz, and Tasuj Faults to the south. Petrographic characteristics such as the occurrence of amphibole in intermediate volcanic rocks, the lack of potassic-ultrapotassic rocks, the whole rock major and trace elements contents as well as the chemical composition of mica and clinopyroxene, suggest that the composition of the parental melt is not the same for the two series of volcanic rocks in this area. The pyroxenite xenoliths occurring in the intermediate volcanic rocks display cumulate texture and are subdivided into four groups based mainly on the modal mineralogy and on the whole rock trace element contents (especially REE). Two groups (Group 1 and 4) have a parental melt similar to that of the intermediate volcanic rocks while the parental melt of Group 2 samples is similar to that of the potassic and ultrapotassic volcanic rocks. Finally, the Group 3 clinopyroxenites differ from those of the other pyroxenite groups and the two series of volcanic rocks.

Estimation of formation temperatures and pressures of clinopyroxene in the different groups of pyroxenite xenoliths and volcanic rocks evidences that the pyroxenite xenoliths of Groups 1, 3, and 4 crystallized at crustal depth ranging from 35 to 39, 20 to 30 and 12 to 40 km, respectively. By comparison, the Group 2 pyroxenite xenoliths formed within the upper mantle at 50–60 km depth. Finally, clinopyroxenes from intermediate volcanic rocks and potassic-ultrapotassic volcanic rocks formed at shallower depths ranging from 2 to12 and 12 to 20 km, respectively.

Acknowledgements This work is a part of the PhD thesis of the first author. Field studies were supported by Tabriz University and the necessary analyses were supported through the Geosciences Environment Toulouse Laboratory (Toulouse University, CNRS, CNES, IRD, UPS, France). We thank Dr. Mohammad Kilzi for his help with the preparation of the analysis.

References

Ackerman L, Spacek P, Medaris G, Hegner E, Svojtka M, Ulrych J (2012) Geochemistry and petrology of pyroxenite xenoliths from Cenozoic alkaline basalts, bohemian massif. J Geosci 57:199–219

Ahankoub M, Jahangiri A, Asahara Y, Moayyed M (2013) Petrochemical and Sr-Nd isotope investigations of A-type granites in the east of Misho, NW Iran. Arab J Geosci 6:4833–4849

Ahmadzadeh G, Jahangiri A, Lentz D, Mojtahedi M (2010) Petrogenesis of Plio-quaternary post-collisional ultrapotassic volcanism in NW of Marand, NW Iran. J Asian Earth Sci 39:37–50

Alavi M (1994) Tectonics of the Zagros orogenic belt of Iran: new data and interpretations. Tectonophysics 220:211–238

Alavi M (2004) Regional stratigraphy of the Zagros folded-thrust belt of Iran and its proforeland evolution. Amer J Sci 304:1–20

Arima M, Edgar AD (1981) Substitution mechanisms and solubility of titanium in phlogopites from rocks of probable mantle origin. Contrib Mineral Petrol 77:288–295

Baker JA, Menzies MA, Thirlwall MF, Macpherson CG (1997) Petrogenesis of quaternary intraplate volcanism, Sana'a, Yemen: implications for plume–lithosphere interaction and polybaric melt hybridization. Petrology 38:1359–1390

Barrat JA, Yamaguchi A, Greenwood RC, Bohn M, Cotten J, Benoit M, Franchi IA (2007) The Stannern trend eucrites: contamination of main group eucritic magmas by crustal partial melts. Geochim Cosmochim Acta 71:4108–4124

Barth MG, McDonough WF, Rudnick RL (2000) Tracking the budget of Nb and Ta in the continental crust. Chem Geol 165:197–213

Bazargani A (2014) Petrography and petrology of subvocanic rocks in Tabakh Daghi dome of South West Marand, NW Iran. Dissertation, University of Tabriz (in Persian)

Berberian M, King GCP (1981) Towards a palegeography and tectonic evolution of Iran. Can J Earth Sci 18:210–265

Best MG, Christiansen EH (2001) Igneous petrology. Blackwell, London

Bondi M, Morten L, Nimis P, Rossi PL, Tranne CA (2002) Megacrysts and mafic–ultramafic xenolith-bearing ignimbrites from Sirwa volcano, Morocco: phase petrology and thermobarometry. Mineral Petrol 75:203–221

Boudier F, Ceuleneer G, Nicolas A (1988) Shear zones, thrusts and related magmatism in the Oman ophiolite: initiation of thrusting on an oceanic ridge. Tectonophysics 151:275–296

Boynton WV (1984) Geochemistry of the rare earth elements: meteorite studies. In: Henderson P (ed) Rare earth element geochemistry. Elsevier, Amsterdam, pp 63–114

Coleman RG (1971) Plate tectonic emplacement of upper mantle peridotites along continental edges. J Geophys Res 76:1212–1222

Cotten J, Le Dez A, Bau M, Maury R, Dulsky P, Fourcade S, Bohn M, Brousse R (1995) Origin and anomalous rare-earth element and yttrium enrichments in subaerially exposed basalts: evidence from French Polynesia. Chem Geol 119:115–138

Dehghan GA, Makris T (1984) The gravity field and crustal structure of Iran. Neues Jb Geol Paläontol Abh 168:215–229

Downes H (1993) The nature of the lower continental crust of Europe; petrological and geochemical evidence from xenoliths. Phys Earth Planet Inter 79:195–218

Egorova VV, Volkova NI, Shelepaev RA, Izokh AE (2006) The lithosphere beneath Sangilen plateau, Siberia: evidence from peridotite, pyroxenite and gabbro xenoliths from alkaline basalts. Mineral Petrol 88:419–441

Emami H (1981) Geologie de la region de Qom-Aran (Iran) contribution a l'etude denamique et geochemique du volcanisme Teriaire del' Iran centaral. Dissertation, University of Grenoble

Farhoudi G (1978) A comparison of Zagros geology to island arcs. Geology 86:323–334

Fitton JG, James D, Leeman WP (1991) Basic magmatism associated with late Cenozoic extension in the western United States: compositional variations in space and time. J Geophys Res 96(B8):13693–13711

Gertisser R, Keller J (2000) From basalt to dacite: origin and evolution of the calc alkaline series of Salina, Aeolian arc, Italy. Contrib Mineral Petrol 139:607–626

Ghasemi A, Talbot CJ (2006) A new tectonic scenario for the Sanandaj-Sirjan zone (Iran). J Asian Earth Sci 26:683–693

Gill JB (1981) Orogenic andesites and plate tectonics. Springer, Berlin

Gonzaga RG, Lowry D, Jacob DE, LeRoex A, Schulze D, Menzies MA (2010) Eclogites and garnet pyroxenites: similarities and differences. J Volcanol Geotherm Res 190:235–247

Green NL (2006) Influence of slab thermal structure on basalt source regions and melting conditions: REE and HFSE constraints from the garibaldi volcanic belt, northern Cascadia subduction system. Lithos 87:23–49

Griffin WL, O'Reilly SY, Ryan CG (1999) The composition and origin of sub-continental lithospheric mantle. In: Fei Y, Berth CM, Mysen BO, (eds), Mantle petrology: field observations and high-pressure experimentation; A Tribute to Francis R. (Joe) Boyd. Geochem Soc Spec Publ 6:13–45

Hart SR, Gerlach DC, White WM (1986) A possible new Sr-Nd-Pb mantle array and consequences for mantle mixing. Geochim Cosmochim Acta 50:1551–1557

Henry DJ (1981) Sulfide-silicate relations of the staurolite grade pelitic schists, Rangeley quadrangle, Maine. Dissertation, University of Wisconsin-Madison

Hess PC (1989) Origin of igneous rocks. Harvard, London

Himmelberg GR, Loney RA (1995) Characteristics and petrogenesis of Alaskan-type ultramafic-mafic intrusions, Southeastern Alaska, U.S. Geol Surv Prof Paper, pp 1–47

Ho KS, Chen JC, Smith AD, Juang WS (2000) Petrogenesis of two groups of pyroxenite from Tungchihsu Penghu Islands Taiwan Strait: implications for mantle metasomatism beneath SE China. Chem Geol 167:355–372

Hofmann A, Jochum K, Seufert M, White M (1986) Nb and Pb in oceanic basalts: new constraints on mantle evolution. Earth Planet Sci Lett 33:33–45

Jahangiri A (2007) Post-collisional Miocene adakitic volcanism in NW Iran: geochemical and geodynamic implications. J Asian Earth Sci 30:433–447

Kelemen PB, Dick HJB, Quick JE (1992) Formation of harzburgite by pervasive melt/rock reaction in the upper mantle. Nature 358:635–641

Kheirkhah M, Allen MB, Emami M (2009) Quaternary syn-collision magmatism from the Iran/Turkey borderlands. J Volcanol Geotherm Res 182:1–12

Khezerlou A, Amini S, Moayyed M (2008) Petrology, geochemistry and mineral chemistry of potassic and ultrapotassic rocks of north West Marand, NW Iran. Kharazmi Science 3:183–204 (in Persian)

Kieffer B, Arndt N, Lapierre H et al (2004) Flood and shield basalts from Ethiopia: magmas from the African superswell. Petrology 45:793–834

Koohestani H, Ghaderi M, Emami MH et al (2013) Geochemistry whole rocks and Sr and Nd isotopes from host volcanic rocks of Ag and Au in Chahzard, Uromieh-Dokhtar arc. Geology Science 90:9–24 (in Persian)

Le Bas MJ, Le Maître RW, Streckeisen A, Zanettin B (1986) A chemical classification of volcanic rocks based on the total alkali-silica diagram. Petrology 27:745–750

Leake BE, Woolley AR, Arps CES et al (1997) Nomenclature of amphiboles: report of the subcommittee on amphiboles of the international mineralogical association, commission on new minerals and mineral names. Can Mineral 35:219–246

McDonough WF, Frey FA (1989) Rare earth elements in upper mantle rocks. In: Lipin BR, Mckay GA (eds) Geochemistry and mineralogy of rare earth elements, Rev Mineral, vol 21, pp 99–145

McDonough WF, Sun SS, Ringwood AE, Jagoutz E, Hofmann AW (1992) Potassium, rubidium and cesium in the earth and moon and the evolution of the mantle of the earth. Geochim Cosmochim Acta 56:1001–1012

Medaris LG Jr, Jelinek E, Beard BL, Valley JW, Spicuzza MJ, Strnad L (2013) Garnet pyroxenite in the Biskupice peridotite, bohemian massif: anatomy of a Variscan high-pressure cumulate. J Geosci 58:3–19

Moayyed M, Hosseinzadeh G (2012) Petrography and petrology of A-type granitoids in east of Mishu (Iran) with a view on the importance of geodynamic. Crystallography and Mineralogy 19:115–130 (in Persian)

Moayyed M, Moazzen M (2002) A new view to the Paleo-Tethys suture line position in Iran. Geological Society 9:716–717 (in Persian)

Moradian A, Peacock SM, Rushmer T (1997) Geochemistry, geochronology and petrography of feldspathoid bearing rocks in Urumieh-Dokhtar Volcanic Belt, Iran. Dissertation, University of Wollongong, Australia

Morimoto N, Kitamura M (1983) Q-J diagram for classification of pyroxenes. J Japan Assoc Min Petrol Econ Geol 78:14 (in Japanese)

Morimoto N, Fabrise J, Ferguson A et al (1988) Nomenclature of pyroxenes. Mineral Mag 52:535–555

Nachit H, Ibhi A, Abia EH, Ohoud MB (2005) Discrimination between primary magmatic biotites, reequilibrated biotites and neoformed biotites. Compt Rendus Geosci 337:1415–1420

Nasir S, Al-Sayigh A, Alharthy A, Al-Lazki A (2006) Geochemistry and petrology of tertiary volcanic rocks and related ultramafic xenoliths from the central and eastern Oman Mountains. Lithos 90:249–270

Nicolas A (1989) Structures in ophiolites and dynamics of oceanic lithosphere. Kluwer, Dordrecht

Orejana D, Villaseca C, Paterson BA (2006) Geochemistry of pyroxenitic and hornblenditic xenoliths in alkaline lamprophyres from the Spanish central system. Lithos 86:167–196

Pang KN, Chung SL, Zarrinkoub MH, Lin YC, Lee HY, Lo CH, Khatib MM (2013) Iranian ultrapotassic volcanism at ~11 Ma signifies the initiation of postcollisional magmatism in the Arabia-Eurasia collision zone. Terra Nov. 25:405–413

Patchett PJ, Chase CG (2002) Role of transform continental margins in major crustal growth episodes. Geology 30:39–42

Pearce JA, Norry MJ (1976) Petrogenetic implications of Ti, Zr, Y, and Nb variations in volcanic rocks. Contrib Mineral Petrol 69:33–47

Peccerillo A, Taylor SR (1976) Geochemistry of Eocene calc-alkaline volcanic rocks in the Kastamonu area, northern Turkey. Contrib Mineral Petrol 58:63–81

Pin C, Santos Zalduegui JF (1997) Sequential separation of light rare-earth elements, thorium and uranium by miniaturized extraction chromatography: application to isotopic analyses of silicate rocks. Anal Chem Acta 339:79–89

Platevoet B, Elitok O, Guillou H et al (2014) Petrology of quaternary volcanic rocks and related plutonic xenoliths from Gölcük volcano, Isparta angle, Turkey: origin and evolution of the high-K alkaline series. J Asian Earth Sci 92:53–76

Porreca C, Selverstone J, Samuels K (2006) Pyroxenite xenoliths from the Rio Puerco volcanic field, New Mexico: melt metasomatism at the margin of the Rio Grande rift. Geosphere 2:333–351. doi:10.1130/GES00058.1

Putirca K, Johnson M, Kinzler R, Longhi J, Walker D (1996) Thermobarometry of mafic igneous rocks based on clinopyroxene-liquid equilibria, 0-30 kbar. Contrib Mineral Petrol 123:92–108

Putirka K (2008) Thermometers and barometers for volcanic systems. Mineral Soc America 69:61–120

Ricou LE (1971) Le croissant ophiolitique péri-arabe, une ceinture de nappes mise en place au crétacé supérieur. Rev Géogr Phys Géol Dyn 13:327–350

Rollinson H (1993) Using geochemical data: evalution, presentation, interpretation. Longman, New York

Rudnick RL, Gao S (2003) Composition of the continental crust. In: Rudnick RL (ed) The crust, Treatise on Geochemistry 3. Elsevier-Pergamon, Oxford, pp 1–64

Saadat S, Stern CR (2012) Petrochemistry of a xenolith-bearing Neogene alkali olivine basalt from northeastern Iran. J Volcanol Geotherm Res 225–226:13–29

Saunders AD, Norry MJ, Tarney J (1991) Fluid influence on the trace element composition of subduction zone magmas. Phil Trans R Soc London 335:377–392

Searle MP, Cox J (1999) Tectonic setting, origin and obduction of the Oman ophiolite. Geol Soc Am Bull 111:104–122

Shafaii Moghadam H, Ghorbani G, Zaki Khedr M et al (2013) Late Miocene K-rich volcanism in the Eslamieh peninsula (Saray), NW Iran: Implications for geodynamic evolution of the Turkish-Iranian High Plateau. Gondwana Res. doi:10.1016/j.gr

Sial AN, Ferreira VP, Fallick AE, Jeronimo M, Cruz M (1998) Amphibole-rich clots in calcalkalic granitoids in the Borborema province northeastern Brazil. J S Am Earth Sci 11:457–471

Speer JA (1984) Mica in igneous rocks. In: bailey SW (ed) micas. Rev Mineral 13:299–356

Stöcklin J (1974) Possible ancient continental margins in Iran. In: Burk CA, Drake CL (eds) The geology of continental margins. Springer, New York, pp 873–887

Stöcklin J (1977) Structural correlation of the alpine ranges between Iran and Central Asia. Mem Ser Soc Geol France 8:333–353

Whitechurch H, Juteau T, Montigny R (1984) The eastern Mediterranean ophiolites (Turkey, Syria, Cyprus): their contribution to the history of the neo-Tethys. In: Dixon JE, Robertson AHF (eds) The geological evolution of the eastern Mediterranean, Geol Soc London Spec Publ, vol 17, pp 425–441

Willson M (1989) Igneous petrogenesis; a global tectonic approach. Unwin Hyman, London

Wood IA, Joron LL, Treuil M, Norry L, Tarney J (1979) Elemental and Sr isotope variation in basic lavas from Iceland and surrounding ocean floor. Contrib Mineral Petrol 70:319–339

Xu Y (2002) Evidence for crustal components in the mantle and constraints on crustal recycling mechanisms: pyroxenite xenoliths from Hannuoba, North China. Chem Geol 182:301–322

Yang JH, Chung SL, Wilde SA, Wu F, Chu MF, Lo CH, Fan H (2005) Petrogenesis of post-orogenic syenites in the Sulu orogenic belt, East China: geochronological, geochemical and Nd–Sr isotopic evidence. Chem Geol 214:99–125

Ying J, Zhang H, Tang Y, Su B, Zhou X (2013) Diverse crustal components in pyroxenite xenoliths from Junan, Sulu orogenic belt: implications for lithospheric modification invoked by continental subduction. Chem Geol 356:181–192

Zhang HF, Nakamura E, Kobayashi K, Ying JF, Tang YJ (2010) Recycled crustal melt injection into lithospheric mantle: implication from cumulative composite and pyroxenite xenoliths. Int J Earth Sci 99:1167–1186

Zindler A, Hart SR (1986) Chemical geodynamics. Annu Rev Earth Planet Sci 14:493–571